Components of neuronal chloride transport in rat and human neocortex

Rudolf A. Deisz[1], Thomas-N. Lehmann[2], Peter Horn[3], Christoph Dehnicke[4] and Robert Nitsch[5]

[1]*Institute of Cell Biology and Neurobiology, Center for Anatomy, Charité – Universitätsmedizin Berlin, Berlin, Germany*
[2]*Klinik für Neurochirurgie, Helios Klinikum Bad Saarow, Bad Saarow, Germany*
[3]*Department of Neurosurgery, Charité – Universitätsmedizin Berlin, Berlin, Germany*
[4]*Epilepsie-Zentrum Berlin-Brandenburg, Evangelisches Krankenhaus Königin Elisabeth Herzberge, Berlin, Germany*
[5]*Institute for Microanatomy and Neurobiology, University Medical Center Mainz, Mainz, Germany*

Non-technical summary The inhibitory neurotransmitter GABA activates two distinct receptors of which the $GABA_A$ receptor is mainly a Cl^- conducting ion channel. The proper functioning of inhibition at the $GABA_A$ receptor depends on the ionic gradient prevailing during receptor activation, and in epilepsy there is an aberrant Cl^- gradient. Using rat and human cortical neurones and pharmacological inhibitors, we calculated the contributions of neuronal Cl^- extrusion by the Na^+–K^+–$2Cl^-$ transporter NKCC1, the K^+-coupled Cl^- transporter KCC2 and the voltage-gated Cl^- channel ClC2. We found that KCC2 is the major route of Cl^- extrusion and that reduced KCC2 Cl^- extrusion is likely to be the initial step of disturbed Cl^- regulation. The results contribute to our understanding of epilepsy.

Abstract Considerable evidence indicates disturbances in the ionic gradient of $GABA_A$ receptor-mediated inhibition of neurones in human epileptogenic tissues. Two contending mechanisms have been proposed, reduced outward and increased inward Cl^- transporters. We investigated the properties of Cl^- transport in human and rat neocortical neurones (layer II/III) using intracellular recordings in slices of cortical tissue. We measured the alterations in reversal potential of the pharmacologically isolated inhibitory postsynaptic potential mediated by $GABA_A$ receptors ($IPSP_A$) to estimate the ionic gradient and kinetics of Cl^- efflux after Cl^- injections before and during application of selected blockers of Cl^- routes (furosemide, bumetanide, 9-anthracene carboxylic acid and Cs^+). Neurones from human epileptogenic cortex exhibited a fairly depolarized reversal potential of $GABA_A$ receptor-mediated inhibition (E_{IPSP-A}) of -61.9 ± 8.3 mV. In about half of the neurones, the $E_{IPSP\text{-}A}$ averaged -55.2 ± 5.7 mV, in the other half, 68.6 ± 2.3 mV, similar to rat neurones (-68.9 ± 2.6 mV). After injections of Cl^-, $IPSP_A$ recovered in human neurones with an average time constant (τ) of 19.0 ± 9.6 s (rat neurones: 7.2 ± 2.4 s). We calculated Cl^- extrusion rates ($1/\tau$) via individual routes from the τ values obtained in different experimental conditions, revealing that, for example, the K^+-coupled Cl^- transporter KCC2 comprises 45.3% of the total rate in rat neurones. In human neurones, the total rate of Cl^- extrusion was 63.9% smaller, and rates via KCC2, the Na^+–K^+–$2Cl^-$ transporter NKCC1 and the voltage-gated Cl^- channel ClC were smaller than in rat neurones by 80.0%, 61.7% and 79.9%, respectively. The rate via anion exchangers conversely was 14.4% larger in human than in rat neurones. We propose that (i) KCC2 is the major route of Cl^- extrusion in cortical

DOI: 10.1113/jphysiol.2010.201830

neurones, (ii) reduced KCC2 is the initial step of disturbed Cl^- regulation and (iii) reductions in KCC2 contribute to depolarizing $E_{IPSP\text{-}A}$ of neurones in human epileptogenic neocortex.

(Resubmitted 29 October 2010; accepted after revision 31 December 2010; first published online 4 January 2011)
Corresponding author R. A. Deisz: Institute of Cell Biology and Neurobiology, Center for Anatomy, Charité – Universitätsmedizin Berlin, Philippstr 12, 10115 Berlin, Germany. Email: rudolf.deisz@charite.de

Abbreviations AE, anion exchanger; CD-ACSF, ACSF containing CNQX and D-APV; CDC-ACSF, ACSF containing CNQX, D-APV and CGP 55845A; ClC, voltage-gated Cl^- channels; $E_{IPSP\text{-}A}$, reversal potential of $GABA_A$ receptor-mediated inhibition; E_m, resting membrane potential; HENC, human epileptogenic neocortex; $IPSP_A$, inhibitory postsynaptic potential mediated by $GABA_A$ receptors; KCC2, neuronal isoform of a K^+-coupled Cl^- transporter; NKCC1, Na^+–K^+–$2Cl^-$ transporter.

Introduction

Synaptically released GABA activates two molecularly and pharmacologically distinct receptors, coined $GABA_A$ and $GABA_B$ (see Teichgräber *et al.* 2009). Disturbance of $GABA_A$ receptor-mediated inhibition is well known to contribute to hyperexcitability in rodent models of epilepsy. Early experiments *in vitro* demonstrated that blockade of $GABA_A$ receptors with antagonists generates paroxysmal depolarizations resembling *in vivo* epileptogenic activity (Gutnick *et al.* 1982). Indeed, a decreased $GABA_A$ receptor function, via altered subunit expression, was shown in the hippocampus of a rodent model of epilepsy (e.g. Rice *et al.* 1996). Conversely, several drugs used in epilepsy therapy (e.g. benzodiazepines, phenytoin) augment $GABA_A$ receptor function (Polc & Haefely, 1976; Deisz & Lux, 1977; Aickin *et al.* 1981; Granger *et al.* 1995).

However, the proper function of GABAergic transmission depends not only on intact receptors and sufficient GABA release, but also on the ionic gradient prevailing during receptor activation. The reversal potential of $GABA_A$ receptor-mediated responses ($E_{IPSP\text{-}A}$) is dominated by the Cl^- gradient across the neuronal membrane (Deisz & Lux, 1982; Thompson *et al.* 1988*a*). However, the partial HCO_3^- permeability of $GABA_A$ receptors (Bormann *et al.* 1987; Kaila *et al.* 1993), with a HCO_3^- reversal potential of about −10 mV (see Alvarez-Leefmans, 1990), causes a disparity (about 10 mV) between the Cl^- gradient (E_{Cl}) and the $E_{IPSP\text{-}A}$ in the neocortex (Kaila *et al.* 1993). In various neurones, $[Cl^-]_i$ is maintained below passive distribution by an NH_4^+-sensitive (Lux, 1971; Llinás *et al.* 1974; Raabe & Gumnit, 1975; Aickin *et al.* 1982; Deisz & Lux, 1982; Thompson *et al.* 1988a; Williams & Payne, 2004) and furosemide-sensitive Cl^- outward transport mechanism (Deisz & Lux, 1982; Misgeld *et al.* 1986; Thompson *et al.* 1988*a*; Titz *et al.* 2006), coupled to K^+ (Aickin *et al.* 1982; Deisz & Lux, 1982). A K^+-coupled Cl^- transporter was cloned, revealing a neurone-specific isoform, KCC2 (Payne *et al.* 1996), which is the molecular substrate for K^+-coupled Cl^- outward transport in central neurones (for review, see Gamba, 2005).

Previous evidence suggests that relatively high $[Cl^-]_i$ depends on inward transport in some peripheral neurones (for brief review see Delpire, 2000). The molecular basis for this is probably the NKCC family of Na^+/K^+-coupled Cl^- transporters (for review, see Gamba, 2005). More recent evidence indicates that the isoform NKCC1 mediates inward Cl^- transport in central neurones (e.g. Dzhala *et al.* 2005; Achilles *et al.* 2007; Brumback & Staley, 2008). On the other hand, the selective antagonist bumetanide reduces Cl^- outward transport in the neocortex (Thompson *et al.* 1988*b*). Nevertheless, these two potentially opposing transport mechanisms play a crucial role during postnatal development (for review see Ben-Ari, 2002). Between postnatal days 11 and 16 a slow Cl^- outward transport and an $E_{IPSP\text{-}A}$ less negative than resting membrane potential (E_m) were shown in the rat neocortex (Luhmann & Prince, 1991), consistent with a presence of NKCC1 at a fairly low rate (Achilles *et al.* 2007). Molecular analysis revealed that NKCC1 expression in the neocortex is much higher until postnatal day 10 (about 1500%) compared with the adult level and then progressively declines. Conversely, expression of KCC2 is relatively low at postnatal day 10 (about 10% *vs.* adult) and increases to adult levels (Dzhala *et al.* 2005). The postnatal increase in KCC2 expression (Rivera *et al.* 1999; Dzhala *et al.* 2005) shifts the polarity of GABAergic responses from depolarization to the mature (i.e. inhibitory) behaviour of cortical $E_{IPSP\text{-}A}$ close to E_m (Connors *et al.* 1988; Thompson *et al.* 1988*a*; Deisz & Prince, 1989; Kaila *et al.* 1993).

Other pathways have to be considered in addition to these two transporters. The family of voltage-activated Cl^- channels (ClC; Jentsch *et al.* 1990; Thiemann *et al.* 1992) comprises nine isoforms, some of which are present in the neocortex. Most of these channels are located at endosomal or vesicular membranes (ClC3–7), and hence the predominant channel in plasma membranes is probably ClC2 (Jentsch *et al.* 2005). Reduced ClC2 expression has been implicated in causing depolarizing GABA responses in the hippocampus during development (Mladinic *et al.* 1999), yet the role of ClC isoforms in maintaining low $[Cl^-]_i$ has not been definitively established. Finally, anion exchangers (AE) are expressed in the CNS (Havenga

et al. 1994) but little is known about their role in Cl^- homeostasis.

Together, at least five different pathways participate in Cl^- movements across neuronal membranes in cortical neurones, namely the $GABA_A$ receptors, KCC2, NKCC1, AE and ClC2. The relative contribution of these pathways to the normal function of GABAergic inhibition is poorly understood in the rodent cortex let alone in the human neocortex. Detailed analysis of the components of Cl^- homeostasis is hampered partly due to the lack of potent and selective pharmacological tools. For instance, furosemide, a widely used blocker of neuronal Cl^- transport (Deisz & Lux, 1982; Misgeld *et al.* 1986; Thompson *et al.* 1988*a*; DeFazio *et al.* 2000; Williams & Payne, 2004), decreases K^+-coupled Cl^- outward transport and thus increases $[Cl^-]_i$ (Deisz & Lux, 1982). However, furosemide also blocks AE of erythrocytes (Brazy & Gunn, 1976) and NKCC1 (see Russell, 2000 for review).

Mounting evidence indicates that the ionic gradient of inhibition is disturbed in human epileptogenic tissues. Depolarizing $GABA_A$ receptor-mediated responses have been reported in neocortical (Deisz *et al.* 1998) and hippocampal tissues (Cohen *et al.* 2002; Huberfeld *et al.* 2007) obtained from epilepsy surgery. However, the mechanisms by which $GABA_A$ receptor-mediated responses are converted into depolarizations are controversial. In the neocortex, reductions of KCC2 (Deisz *et al.* 1998) or an up-regulation of NKCC1 (Palma *et al.* 2006) have been proposed, either of which may shift the balance between the two opposing directions of Cl^- transport, thus possibly setting the $E_{IPSP\text{-}A}$ to more depolarized values.

We evaluated possible mechanisms contributing to altered Cl^- homeostasis in human cortical neurones in epilepsy surgery tissue (HENC neurones). Parallel experiments were carried out in rat cortical neurones to establish the effects of several drugs on Cl^- homeostasis, allowing us to estimate the relative contribution of various pathways to Cl^- efflux from rat and HENC neurones.

Methods

Human and rat cortical tissue

The experiments were approved by the ethics committee of the Charité (30.9.1997) and all patients provided informed consent for use of their tissues in adherence with the *Declaration of Helsinki*. A total of 96 resections (43 female and 53 male patients) were investigated. On average, the patients were (means ± S.D.) 35.0 ± 13.8 years old and suffered epilepsy since the age of 15.0 ± 12.0 years, i.e. for 19.7 ± 13.6 years. Tissues from patients with temporal lobe epilepsy (TLE with or without ammon's horn sclerosis) consisting mainly of the frontal pole of the temporal lobe comprised the largest group of resections (70%). Epileptogenic tissues from other sites were less frequent (frontal lobe epilepsy 4%) and some tissues exhibited also various pathologies (tumour 10%, dysplasia 9%, lesion 7%). For brevity's sake, we refer to neurones from human epileptogenic tissues collectively as HENC neurones.

The procedures have been previously described (Deisz, 1999*b*; Teichgräber *et al.* 2009). In brief, human cortical tissue was collected in the operating theatre and transferred to the laboratory in a cold modified artificial cerebrospinal fluid (mACSF, see below). The tissue was cut into smaller blocks which were subsequently cut into slices (nominally 400 μm) with a vibratome (TPI 1000, St Louis, MO, USA or HM650V, Microm, Walldorf, Germany). The slices were stored at room temperature in beakers filled with artificial cerebrospinal fluid (ACSF, composition see below) equilibrated with 95% O_2–5% CO_2 until used.

Experiments on slices of rat sensorimotor cortex (Wistar, age 30–50 days) were made adhering to accepted guidelines regarding housing and handling of animals (see Deisz, 1999*a*). The experiments were registered at the responsible authority (Landesamt für Arbeitsschutz, Gesundheitsschutz und technische Sicherheit Berlin, T 0206/96). In brief, animals were anaesthetized with ether and decapitated with an animal guillotine. The relevant block of the brain was removed and slices were made using the same methods and maintained under identical conditions as the human tissue slices.

Solutions and drugs

For the transport of the tissue we used cold (about 5°C) mACSF containing (in mM): NaCl 70, KCl 2.5, NaH_2PO_4 1.25, $MgSO_4$ 2, $CaCl_2$ 0.5, $NaHCO_3$ 26, (+)-D-glucose 25 and sucrose 75, equilibrated with 95% O_2–5% CO_2, pH 7.4. For storage of the slices and recording we used a standard ACSF containing (in mM): NaCl 124, KCl 5, NaH_2PO_4 1.25, $MgSO_4$ 2, $CaCl_2$ 2, $NaHCO_3$ 26 and (+)-D-glucose 10, equilibrated with 95% O_2–5% CO_2, pH 7.4. These substances were of analytical grade (Merck, Darmstadt, Germany). The antagonists for the AMPA- and NMDA-type glutamate receptors, CNQX and D-APV (Tocris Bioscience, Bristol, UK or Ascent Scientific, Weston-Super-Mare, UK), were usually applied at 10 and 20 μM, respectively. In some cases the concentrations were increased to 20 and 50 μM. The ACSF containing these two antagonists will be referred to as CD-ACSF. In some experiments we also added 2 μM CGP 55845A ([3-[[(1*S*)-1-(3,4-dichlorophenyl)ethyl]amino]-2-(*S*)-hydroxypropyl](phenylmethyl)phosphinic acid hydrochloride), a potent $GABA_B$ receptor antagonist (kindly provided by Novartis, Basel, Switzerland), to the CD-ACSF, termed CDC-ACSF. We chose CGP 55845A

because it antagonizes not only postsynaptic but also presynaptic $GABA_B$ receptors (Deisz, 1999*a*; Teichgräber *et al.* 2009), hence reducing the frequency-dependent depression of inhibition (Deisz & Prince, 1989). These drugs were added to the ACSF from aqueous stock solutions (stored at −20°C). Furosemide (200 μM) and bumetanide (10 μM or 50 μM; both Sigma, Taufkirchen, Germany) were added directly to the ACSF or CDC-ACSF. Stock solutions of the voltage-gated Cl^- channel blocker 9-anthracene carboxylic acid (9AC; Clark *et al.* 1998) were made with DMSO. The maximal DMSO content in the ACSF was 0.1%.

Recording and stimulation

Individual slices were transferred to a submerged-type recording chamber and perfused with 95 % O_2–5% CO_2-equilibrated ACSF at about 5 ml min^{-1}. Temperature was kept constant at 32°C with a temperature controller (SCTC-20E, npi, Tamm, Germany). Intracellular recordings were carried out in cortical layer II/III neurones with sharp microelectrodes. Neurones were selected if they had a resting membrane potential more negative than −60 mV, action potential (AP) amplitudes >70 mV and input resistances >10 MΩ. Only regularly firing neurones were included; burst-firing neurones (e.g. Deisz, 1996) were only rarely encountered. Pipettes were pulled from filamented borosilicate glass (1.2 mm o.d., 0.8 mm i.d, Hilgenberg, Malsfeld, Germany) with a Brown–Flaming pipette puller (P87, Sutter Instruments, Novato, CA, USA). Electrode resistances ranged from 80 to 100 MΩ when filled with potassium acetate (1 M KAc; Sigma, plus 1 mM KCl titrated to pH 7.2 with acetic acid). In experiments to alter the anion gradient, 1 M KCl (plus 10 mM Hepes titrated to 7.2 with KOH) or 1 M KNO_3 filling solution was used to increase the intracellular anion concentration as previously described (Misgeld *et al.* 1986; Thompson *et al.* 1988a; Luhmann & Prince, 1991). Electrodes were connected to a current-clamp amplifier (SEC-10, npi). Data were digitized online with PC-based acquisition hardware and software (Digidata 1200 system and pCLAMP 9.2; Molecular Devices, Sunnyvale, CA, USA; some early experiments were recorded with the preceding generation of hardware and software).

Bipolar stimulating electrodes (SNEX-200X, Science Products, Hofheim, Germany) positioned in layer I in the vicinity of the recorded neurone were used to elicit synaptic responses. We chose stimulation in layer I rather than layer VI because from this location IPSPs could be evoked before and after pharmacological isolation. Orthodromic stimuli (duration 100 μs, usually 0.2 Hz or below, unless stated otherwise) were delivered using an isolation unit (A.M.P.I., Jerusalem, Israel). All traces shown in the figures were subjected to digital filtering (800 Hz) and truncation of stimulus artefacts.

Families of current injections (steps from −0.5 nA to +0.7 nA, 0.05 nA increment, 600 ms, at 0.2 Hz) were applied to estimate neuronal input resistance, firing properties and AP amplitudes. A second family of current injections was applied with a concomitant orthodromic stimulus (usually 12 V) to evaluate voltage-dependent properties of synaptic potentials and to determine the $E_{IPSP\text{-}A}$. To this end, the linear part of the amplitude–voltage relation was approximated by linear fit.

To ascertain the steady-state condition of the applied drugs, the time course of solution exchange was determined by evaluating the amplitudes of postsynaptic potentials (PSPs) (elicited at 0.1 or 0.05 Hz) during washing in CDC-ACSF. The gradual dwindling of the amplitude on application of CDC-ACSF was approximated by an exponential fit yielding a τ of decay of about 100 s. Thus, measurements commenced 10 min after the start of solution exchange when steady state had been attained.

To evaluate the time course of Cl^- efflux, synaptic potentials were elicited at 0.2 or 0.33 Hz before, during and after iontophoretic injection of Cl^- (0.5, 1 or 2 nA for 0.5 or 1 min). The amplitudes of $IPSP_A$ responses were measured from a window (12–18 ms, usually about 15 ms) after the stimulus (apparent time to peak of the $IPSP_A$). A given time point was kept for all $IPSP_A$ measurements from a neurone, except after pharmacological isolation, then the peak at resting E_m was taken. The decay of amplitude after cessation of iontophoresis was fitted by a single exponential function to determine the kinetics of recovery of $IPSP_A$ amplitudes. To reduce contamination of the $IPSP_A$ by temporally overlapping excitatory postsynaptic potentials (EPSPs) and $GABA_B$ receptor-mediated IPSP ($IPSP_B$), measurements were also carried out in CDC-ACSF. Since the $IPSP_A$ sometimes exhibited considerable fluctuation in amplitude, injections of anions were carried out in triplicate and the data were averaged from a given protocol to obtain a reliable time constant (τ) of $IPSP_A$ amplitude changes.

The time course of $IPSP_A$ changes is too fast (near 7 s; Thompson *et al.* 1988*a*,*b*; Luhmann & Prince, 1991) to be followed by repetitive determinations of $E_{IPSP\text{-}A}$ (30 s for 10 current injections with stimulation at 0.33 Hz). To estimate the changes in $[Cl^-]_i$, we used the following substitute: we determined the driving force of the $IPSP_A$ (E_m–$E_{IPSP\text{-}A}$) and expressed the amplitude as a percentage of the driving force. Assuming linearity between the amplitude and driving force, the peak $IPSP_A$ amplitude after cessation of iontophoresis was used to estimate the maximal $E_{IPSP\text{-}A}$. From this, we calculated $[Cl^-]_i$ using the Goldman–Hodgkin–Katz equation assuming a

permeability ratio Cl^-:HCO_3^- of 1:0.2 (Kaila *et al.* 1993). We refrained from calculating ionic activities and give concentrations throughout.

Assuming first order kinetics, the $IPSP_A$ amplitude recovery was fitted by a single exponential function, the time constant (τ) obtained was used to calculate the rates of Cl^- efflux ($1/\tau$). The difference in rates before and during application of a drug provided an estimate of the transport rate by the affected pathway. With the drugs and experimental conditions employed, the rates of all pathways could be determined using the equations below. The total flux rate of Cl^- extrusion ($\Phi = 1/\tau$ of recovery) is the sum of these four pathways:

$$Cl^-\ \Phi_{total} = \Phi\,KCC2 + \Phi\,NKCC1 + \Phi\,AE + \Phi\,ClC_2, \quad (1)$$

$$\Phi\,NKCC1 : Cl^-\ \Phi = Cl^-\ \Phi_{total} - Cl^-\ \Phi \text{ in bumetanide}, \quad (2)$$

$$\Phi\,ClC_2 : Cl^-\ \Phi = Cl^-\ \Phi_{total} - Cl^-\ \Phi \text{ in 9AC}, \quad (3)$$

$$\Phi\,AE : NO_3^-\ \Phi = NO_3^-\ \Phi_{total} - NO_3^-\ \Phi\,ClC_2, \quad (4)$$

$$\Phi\,KCC2 : Cl^-\Phi = Cl^-\ \Phi_{total} - \Phi\,AE - \Phi\,ClC_2 - \Phi\,NKCC1. \quad (5)$$

Linear and non-linear fits to data points were carried out with Origin 7.1 software (OriginLab Corp., Northampton, MA, USA). Statistical evaluation of the data was usually carried out with a statistics program (Statview, Abacus Concepts Inc., Berkeley, CA, USA), unless stated otherwise. Group differences were evaluated with Student's *t* test for paired or unpaired data as appropriate. To test for a normal distribution of data, or deviation thereof, we used the Kolmogorov–Smirnov test with Lilliefors's significance correction and the Shapiro–Wilk test (PASW statistics program, v. 18, SPSS Inc., Chicago, IL, USA). The number of observations given in the text represents the number of neurones under a particular condition. Since the recording of some neurones was discontinued, the number of observations of subsequent measurements differ. Not all of the various parameters (e.g. $E_{IPSP\text{-}A}$ with KCl-filled electrodes and recovery tau from Cl^- loading) were determined in every neurone, and thus the number of observations of apparently related parameters does not match precisely. Statistical evaluation was, however, carried out on the corresponding pairs. *P* values <0.05 were considered to indicate significant differences. All values are given as means ± S.D. in the text. The vertical bars denote the S.E.M. in all figures.

Some of these data have previously been presented in abstract form (Deisz *et al.* 1998, 2008).

Results

Depolarizing $GABA_A$ receptor-mediated responses

Synaptic responses in HENC neurones consisted of a large depolarization (Deisz, 1999*b*; Teichgräber *et al.* 2009) without the typical sequence of EPSPs and IPSPs observed in rodent cortex (Connors *et al.* 1988; Deisz & Prince, 1989; Kaila *et al.* 1993), i.e. the synaptic responses usually had no discernible $IPSP_A$ component at resting E_m in standard ACSF (Fig. 1*A*). In some neurones the synaptic responses steeply increased with subtle increases in stimulus intensity, similar to pharmacologically induced paroxysmal depolarization shifts (PDSs) in rodent neocortex (Gutnick *et al.* 1982). However, the synaptic responses were, unlike PDSs, often devoid of APs. Therefore, we refer to these compound synaptic responses as depolarizing shifts (DSs). On the other hand, the voltage dependence of these DSs was similar to PDSs, i.e. the membrane potential at the peak of the synaptic response attained almost the same voltage from every potential from which it was elicited, indicating a state of high conductance.

The extrapolated reversal potential of the compound synaptic response (near 15 ms) was a mean of -54.0 ± 10.0 mV ($n = 92$), considerably less negative than in rodent cortical neurones (e.g. Kaila *et al.* 1993). This might be due either to a relative increase in EPSP or alterations in $IPSP_A$. In the presence of CDC-ACSF or CD-ACSF, this reversal potential shifted towards more negative values (Fig. 1*C*), yet a depolarizing component remained in HENC neurones ($E_{IPSP\text{-}A}$: -61.5 ± 8.1 mV; $n = 50$; $P < 0.001$ *vs.* ACSF) with an unaltered resting membrane potential (E_m; ACSF: -71.5 ± 4.6 mV, CD-ACSF or CDC-ACSF: -71.4 ± 4.9 mV; $P > 0.05$). The $E_{IPSP\text{-}A}$ values obtained in CD-ACSF and CDC-ACSF were indistinguishable ($P > 0.05$) and therefore pooled. We considered the possibility of an insufficient block of excitatory amino acid receptors and increased the concentrations of CNQX and D-APV up to 20 and 50 μM in some experiments, but depolarization with a reversal potential near -60 mV persisted. Application of bicuculline at 20 μM reduced the depolarization remaining in CDC-ACSF by about 50% ($n = 1$) and at 50 μM by 85% ($n = 7$, $P < 0.001$), indicating the presence of depolarizing $GABA_A$ receptor-mediated responses (Fig. 1*E* and *F*).

The fairly large S.D. of the reversal potentials in HENC neurones (8.1 mV) indicates a non-homogeneous distribution. The histogram of the data (see Fig. 1*D*) shows at least two distinct peaks in the distribution of the $E_{IPSP\text{-}A}$. Therefore, $E_{IPSP\text{-}A}$ values were segregated into

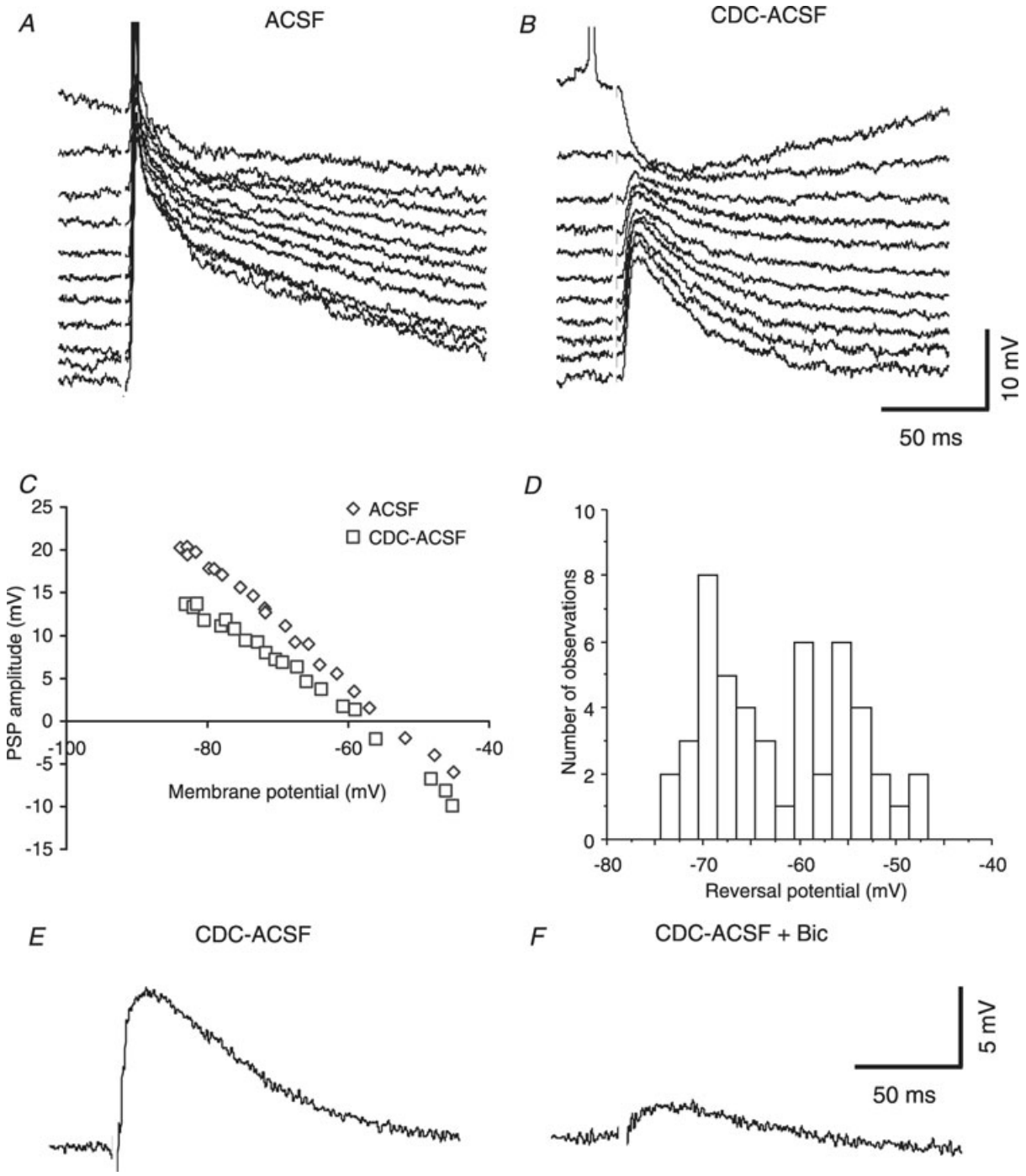

Figure 1. Properties of synaptic responses in HENC neurons
A, voltage traces at various membrane potentials induced by current injection. Orthodromic stimulation (12 V) elicits a fairly large depolarization in control conditions (current injections −0.5 nA to +0.5 nA, 0.1 nA increments; E_m: −72.4 mV; KAc-filled microelectrode). *B*, traces from the same neurone as shown in *A* in the presence of CDC-ACSF, revealing an obvious $IPSP_A$ in the top trace (time-to-peak of ∼25 ms post-stimulus, E_m −72.0 mV, stimulus intensity 12 V). The time of stimulation is obvious from the blanked stimulus artefact here and throughout the figures. *C*, determination of the $E_{IPSP\text{-}A}$ reveals a value of −53.8 mV in control and −59.5 mV in the presence of CDC-ACSF. *D*, histogram of $E_{IPSP\text{-}A}$ values obtained in HENC neurones in the presence of CDC-ACSF. Note the multiple peaks suggesting an inhomogeneous distribution. *E* and *F*, traces of synaptic responses obtained at resting E_m in CDC-ACSF and during addition of 50 μM bicuculline (Bic) as indicated. The incomplete blockade may have been due to excess GABA.

two groups using the mean value plus 2 S.D. of rat neurones as the border (−64.2 mV, see below). Of 50 neurones evaluated, 23 exhibited an $E_{IPSP\text{-}A}$ more negative than −64 mV averaging −68.8 ± 2.3 mV. This value is indistinguishable from that of rat neurones ($P > 0.5$) and close to established data from rodent neurones (e.g. Connors *et al.* 1988). The other group exhibited a less negative $E_{IPSP\text{-}A}$, on average −55.2 ± 5.7 mV ($n = 27$; $P < 0.0001$ *vs.* the other group), indicating a dysfunction of Cl^- homeostasis in about half of the HENC neurones. To verify this difference statistically, we used the Kolmogorov–Smirnov test with Lilliefors's significance correction and the Shapiro–Wilk test, both indicating significant differences between the two subpopulations ($P = 0.017$ and $P = 0.009$, respectively).

Kinetics of Cl^- transients

To delineate the mechanisms contributing to the depolarizing shift in $E_{IPSP\text{-}A}$, we evaluated the properties of Cl^- outward transport using anion injection (Llinás *et al.* 1974; Thompson *et al.* 1988*a*,*b*) and a variety of bath-applied drugs. Before describing the kinetics of Cl^- transients in HENC neurones, we present parallel experiments on rat cortical neurones corroborating and extending previous data from guinea pig cortex under our experimental conditions (Thompson *et al.* 1988*a*,*b*). Furthermore, we compared $E_{IPSP\text{-}A}$ measurements using KAc-filled microelectrodes and KCl-filled microelectrodes, to estimate Cl^- regulation under steady-state conditions.

Kinetics of Cl^- transport in rat cortical neurones

Recordings from rat cortical neurones with KAc-filled microelectrodes yielded an apparent mean $E_{IPSP\text{-}A}$ of −65.5 ± 3.1 mV ($n = 47$) in ACSF and −69.3 ± 2.5 mV in CDC-ACSF ($n = 16$, $P < 0.001$ *vs.* ACSF. E_m was essentially the same in both conditions (control: −72.7 ± 3.7 mV, $n = 47$; CDC-ACSF: −71.9 ± 3.0 mV, $n = 16$; $P > 0.05$). Recordings from rat cortical neurones with KCl-filled microelectrodes usually caused a fairly rapid shift of the $IPSP_A$ (within a few minutes of impalement), merging with the preceding EPSP. The apparent mean $E_{IPSP\text{-}A}$ was −56.2 ± 6.4 mV ($n = 79$), less negative compared to data obtained with KAc-filled microelectrodes ($P < 0.0001$). Pharmacological isolation of the $IPSP_A$ by applying CDC-ACSF caused a significant shift of the $E_{IPSP\text{-}A}$, to a mean −61.4 ± 4.9 mV ($n = 47$). This corresponds to a $[Cl^-]_i$ of 10.2 mM compared with 6.7 mM when recorded in the same condition with KAc-filled electrodes ($P < 0.001$). This indicates that (i) the apparent $E_{IPSP\text{-}A}$ of rat cortical neurones is 'contaminated' by some overlap with the preceding EPSP and (ii) the steady-state elevation of $[Cl^-]_i$ by leakage from the electrode shifts the $E_{IPSP\text{-}A}$ to values near −60 mV, corresponding to an increase of $[Cl]_i$ from 6.7 mM to 10.2 mM.

Current injection (1 nA, 1 min) caused a further increase in the amplitude of $IPSP_A$ near 15 ms post-stimulus, recovering with a τ of 7.9 ± 2.7 s ($n = 84$) to the preceding control value (Fig. 2*A*, *C* and *D*). The recovery τ exhibited no obvious dependence on the magnitude of the preceding Cl^- load (Fig. 2*F*), averaging 7.4 ± 2.3 s ($n = 11$) after small current injections (0.5 nA for 30 s), and 8.0 ± 3.5 s after large current injections (2 nA for 1 min; $n = 16$; $P > 0.05$). This similar recovery of $IPSP_A$ from different loads allowed averaging per neurone, yielding a mean τ of 7.9 ± 2.4 s ($n = 84$).

This τ of recovery may be inaccurate due to alterations in the partly overlapping EPSP, e.g. through the recruiting of voltage-dependent conductances (Deisz *et al.* 1991) or a frequency-dependent depression of IPSPs (Deisz & Prince, 1989). The latter effect may occur at the higher stimulus frequencies necessary to obtain a reliable resolution of the time course. We therefore evaluated the recovery τ of isolated $IPSP_A$ in CDC-ACSF. The time courses in ACSF and in CDC-ACSF were similar (Fig. 2*D*). Injections of 1 nA (1 min) yielded a τ of 7.2 ± 2.5 s ($n = 47$) and 8.9 ± 3.7 s ($n = 12$) after large current injection (2 nA, 1 min; $P > 0.05$), indicating no effect of Cl^- load on the time course of recovery. The τ values of recovery of the $IPSP_A$ amplitude from iontophoretic injections was of a mean 7.2 ± 2.4 s ($n = 47$), similar to measurements in ACSF ($P > 0.05$). The narrow distribution of time constants (Fig. 2*E*) indicates that the kinetics of Cl^- transport are fairly homogeneous in the population of rat neurones investigated.

To estimate the changes in $[Cl^-]_i$ induced by current injection, we calculated the $E_{IPSP\text{-}A}$ and thence $[Cl^-]_i$ from the $IPSP_A$ amplitude after cessation of current injection (see Methods). Injection of 1 nA for 1 min increased $[Cl^-]_i$ from 9.8 ± 2.8 mM to 14.3 ± 5.0 mM ($n = 20$, $P < 0.0001$), i.e. by 4.5 mM. In a subset of these neurones, injections of 1 nA for 1 min increased $[Cl^-]_i$ from 8.5 ± 2. 9 mM to 11.4 ± 3.8 mM ($n = 5$; $P < 0.01$), i.e. by 2.9 mM, and injections of 2 nA for 1 min increased $[Cl^-]_i$ to 15.3 ± 5.6 mM, i.e. by 6.8 mM ($n = 5$; $P < 0.05$ *vs.* 1 nA). The recovery τ was unaltered, averaging 6.3 and 6.5 s for 1 nA and 2 nA, respectively, despite an approximately twofold greater increase of $[Cl^-]_i$.

Pharmacology of Cl^- transport in rat cortical neurones

To evaluate the contribution of individual Cl^- routes, we investigated the effects of selected blockers on steady-state values of $E_{IPSP\text{-}A}$ and on the kinetics of Cl^- extrusion.

Application of furosemide (200 μM) tended to increase the isolated $IPSP_A$ amplitude from 3.3 ± 1.7 mV to 6.4 ± 5.6 mV (see Fig. 3*A*; $n = 7$; $P = 0.052$). The mean

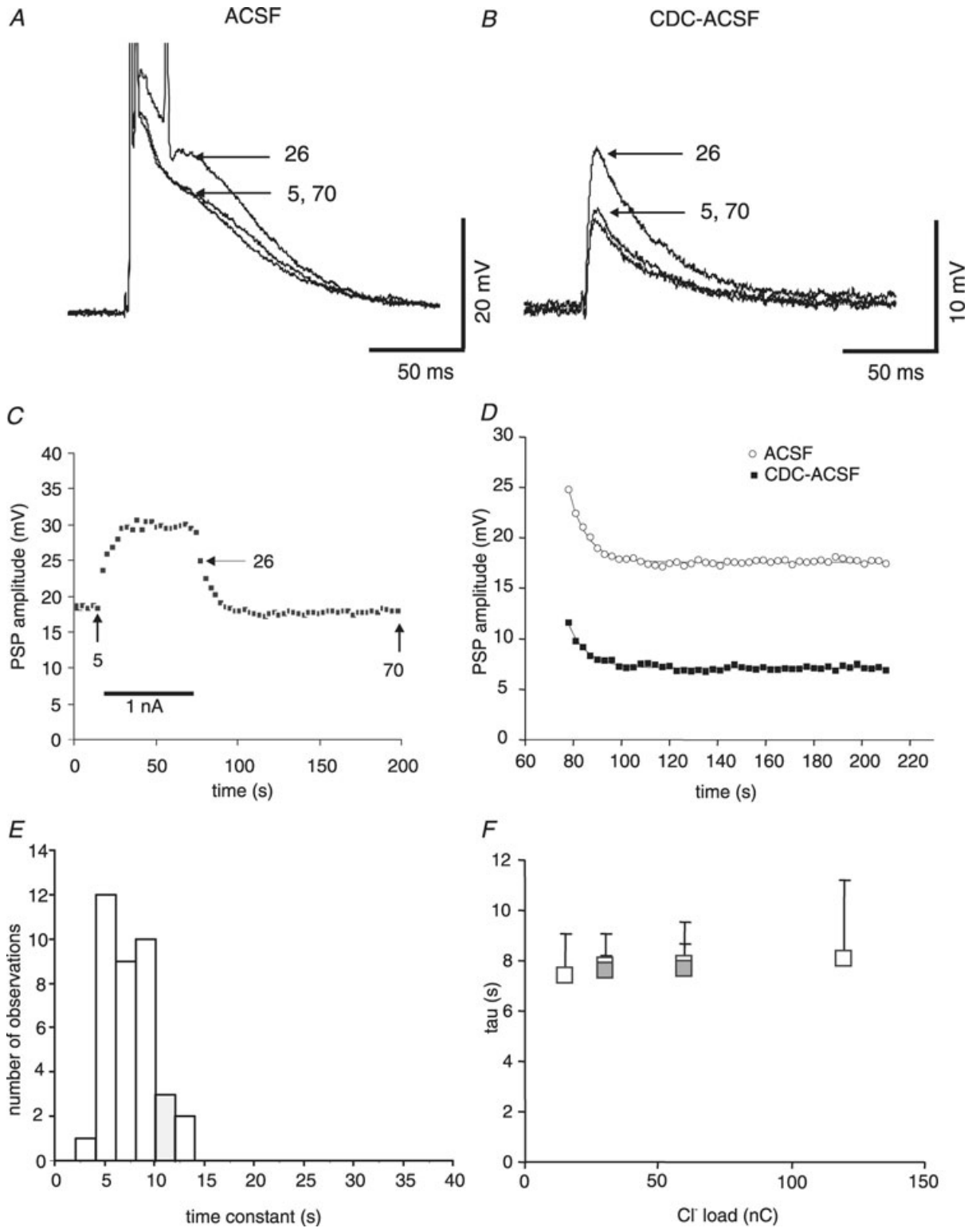

Figure 2. Time course of $IPSP_A$ changes in rat cortical neurones during and after cessation of current injection from a KCl-filled microelectrode

A, traces in ACSF (E_m −73.3 mV) before current injection (sample 5), after end of current injection (sample 26) and after recovery (sample 70). The arrows indicate the point of measurement. *B*, corresponding traces from the same neurone shown in *A* in the presence of CDC-ACSF (E_m −71.0 mV). *C*, plot of the compound PSP amplitudes before, during and after Cl^- injection. The arrows indicate the times of the recordings illustrated in panel *A*. Three consecutive injections from the neurone shown in *A* have been averaged. Note the instantaneous

tau of increase in amplitude (100.2 s; see Fig. 3*B*) was close to the tau of CDC-ACSF effects on PSPs in these neurones (91.7 s), indicating that furosemide took effect quickly. Application of furosemide shifted the $E_{IPSP\text{-}A}$ from -62.9 ± 5.8 mV to -55.4 ± 5.4 mV ($n = 6$, $P < 0.05$; Figs 3*C* and 4*A*), corresponding to a mean increase of $[Cl^-]_i$ from 9.7 mM to 13.9 mM ($n = 5$, $P < 0.05$). The E_m was unaltered ($P > 0.05$, see Fig. 4*A*). Furosemide increased the τ of $IPSP_A$ recovery from 7.1 ± 3.0 s to 16.6 ± 6.7 s ($n = 8$, $P < 0.01$; Fig. 3*D–F*), close to published data from guinea-pig cortex (15.9 s; Thompson *et al.* 1988*a*). The maximal $[Cl^-]_i$ attained after cessation of current injection (1 nA, 1 min) averaged 13.1 ± 4.3 mM in CDC-ACSF and 20.3 ± 6.5 mM in the presence of furosemide. The increases of $[Cl^-]_i$ in CDC-ACSF (4.3 ± 2.9 mM) and furosemide (7.0 ± 4.8 mM) were similar ($n = 5$; $P > 0.05$). During washout of furosemide, the $IPSP_A$ amplitude gradually decreased (from 8.5 to 4.8 mV; tau 258 s, $n = 3$) and the τ of $IPSP_A$ recovery from Cl^- loading returned towards control values (9.3 ± 5.4 s, $n = 3$, $P < 0.05$ *vs.* furosemide and $P > 0.5$ *vs.* preceding control).

Application of 10 or 50 μM bumetanide, a selective blocker of NKCC, increased the amplitude of the isolated $IPSP_A$ during the first 10 min from 3.9 ± 1.6 mV to 6.2 ± 4.9 mV (Fig. 5*D*; $n = 11$, $P < 0.05$). However, in a subset of these neurones, bumetanide had no effect on the $E_{IPSP\text{-}A}$ (CDC-ACSF: -62.8 ± 7.2 mV, bumetanide: -61.5 ± 5.4 mV; $n = 5$; $P > 0.5$; Fig. 4*C*), corresponding to a $[Cl^-]_i$ of 9.9 ± 3.3 mM and 10.3 ± 2.7 mM. The recovery τ of $IPSP_A$ after cessation of Cl^- injection increased from 7.0 ± 1.7 s to 8.6 ± 1.6 s ($n = 12$, $P < 0.001$; see Fig. 5*A–C* and Fig. 10*D*). The effects of 10 μM and 50 μM bumetanide ($n = 6$ each) were similar ($P > 0.05$) and therefore we pooled the data. On washout of bumetanide, the τ of recovery from Cl^- loading returned to control values (6.9 ± 1.7 s, $n = 6$). The maximal $[Cl^-]_i$ after cessation of the current injections averaged 15.6 ± 7.1 mM and 21.3 ± 6.0 mM ($n = 5$; $P < 0.05$) in CDC-ACSF and during addition of bumetanide, respectively. Thus, the injection increased $[Cl^-]_i$ on average by 5.9 ± 4.8 mM in control and 10.9 ± 4.3 mM in the presence of bumetanide ($n = 5$; $P < 0.05$). The significant slowing of recovery together with unaltered $E_{IPSP\text{-}A}$ by bumetanide (see Fig. 4*C*) suggests that NKCC1 plays a minor role in the maintenance of steady state $[Cl^-]_i$ in healthy cortical neurones, but is operating at elevated $[Cl^-]_i$. In addition, it would appear to impede Cl^- loading via iontophoresis, as indicated by the much larger increase of $[Cl^-]_i$ in the presence of bumetanide.

We then tested for involvement of a K^+-dependent Cl^- extrusion by evaluating the effects of reduced $[K^+]_o$ on the kinetics of recovery from Cl^- loading. Reducing $[K^+]_o$ by half (equimolar replacement by 2.5 mM Na^+; both ACSFs containing the CDC additions) reduced the τ of $IPSP_A$ recovery from 8.9 ± 2.3 s to 7.4 ± 2.3 s ($n = 13$, $P < 0.01$; Fig. 6*D*). The reduction of $[K^+]_o$ also caused a hyperpolarizing shift in the $E_{IPSP\text{-}A}$ from -59.3 ± 1.4 mV to -66.2 ± 5.5 mV ($n = 3$). The acceleration of recovery and shift of $E_{IPSP\text{-}A}$ confirmed that the K^+ gradient affects the rate of Cl^- extrusion and steady-state level of $[Cl^-]_i$ in rat cortical neurones. A further test of the involvement of K^+-coupled transporters was made by evaluating the effects of Cs^+, known to have an impact on Cl^- homeostasis (Aickin *et al.* 1982; Kakazu *et al.* 1999; Williams & Payne, 2004). Replacing half of $[K^+]_o$ with 2.5 mM Cs^+ caused a marked increase in the recovery τ (Fig. 6*A–C*), from 7.1 ± 3.0 s to 12.2 ± 4.5 s ($n = 5$, $P < 0.05$ *vs.* 5 mM K^+, Fig. 6*D*).

To estimate the contribution of other Cl^- pathways, namely Cl^-/HCO_3^- exchangers (the AE gene family; Havenga *et al.* 1994) and ClC2 (see Fahlke, 2001), we determined the kinetics of recovery of $IPSP_A$ amplitudes following NO_3^- injections. We chose NO_3^- because it is permeant through the $GABA_A$ receptors (Bormann *et al.* 1987), yet is extruded much more slowly than Cl^- (Thompson *et al.* 1988*b*). Following NO_3^- injection, the amplitudes of $IPSP_A$ recovered fairly slowly to preceding control values (Fig. 7*A–D*). In control ACSF the compound synaptic potentials recovered with a τ of 20.5 ± 9.9 s ($n = 19$, $P < 0.0001$ *vs.* Cl^- injection in ACSF). Similar values were obtained in CDC-ACSF, where the τ averaged 21.1 ± 6.1 s ($n = 17$, $P > 0.05$ *vs.* ACSF; $P < 0.0001$ *vs.* Cl^- injection in CDC-ACSF). To test whether the NO_3^- (i.e. unselective) pathway involves AE, we applied furosemide. Bath application of furosemide (200 μM in CDC-ACSF) considerably increased the recovery τ of $IPSP_A$ following NO_3^- injections to 28.6 ± 4.6 s ($n = 3$).

increase in amplitude due to the step hyperpolarization induced by current injection. *D*, determination of the time constant of $IPSP_A$ amplitude recovery. Applying exponential fits to the data points revealed tau values of 7.5 s in control ACSF (open symbols) and 7.9 s in CDC-ACSF (filled symbols). *E*, histogram of the tau values of $IPSP_A$ recovery in rat neurones in the presence of CDC-ACSF, indicating a fairly homogeneous distribution. *F*, plot of the time constant of recovery from various Cl^- loads. The amount of injected Cl^- has been plotted as charge (nA × time). The open symbols represent data obtained with injections of 15 nC ($n = 11$), 30 nC ($n = 22$), 60 nC ($n = 84$) and 120 nC ($n = 16$). The filled symbols represent data obtained with the same charge applied with different parameters (30 nC by 0.5 nA for 60 s ($n = 11$) and 60 nC by 2 nA 30 s ($n = 22$)).

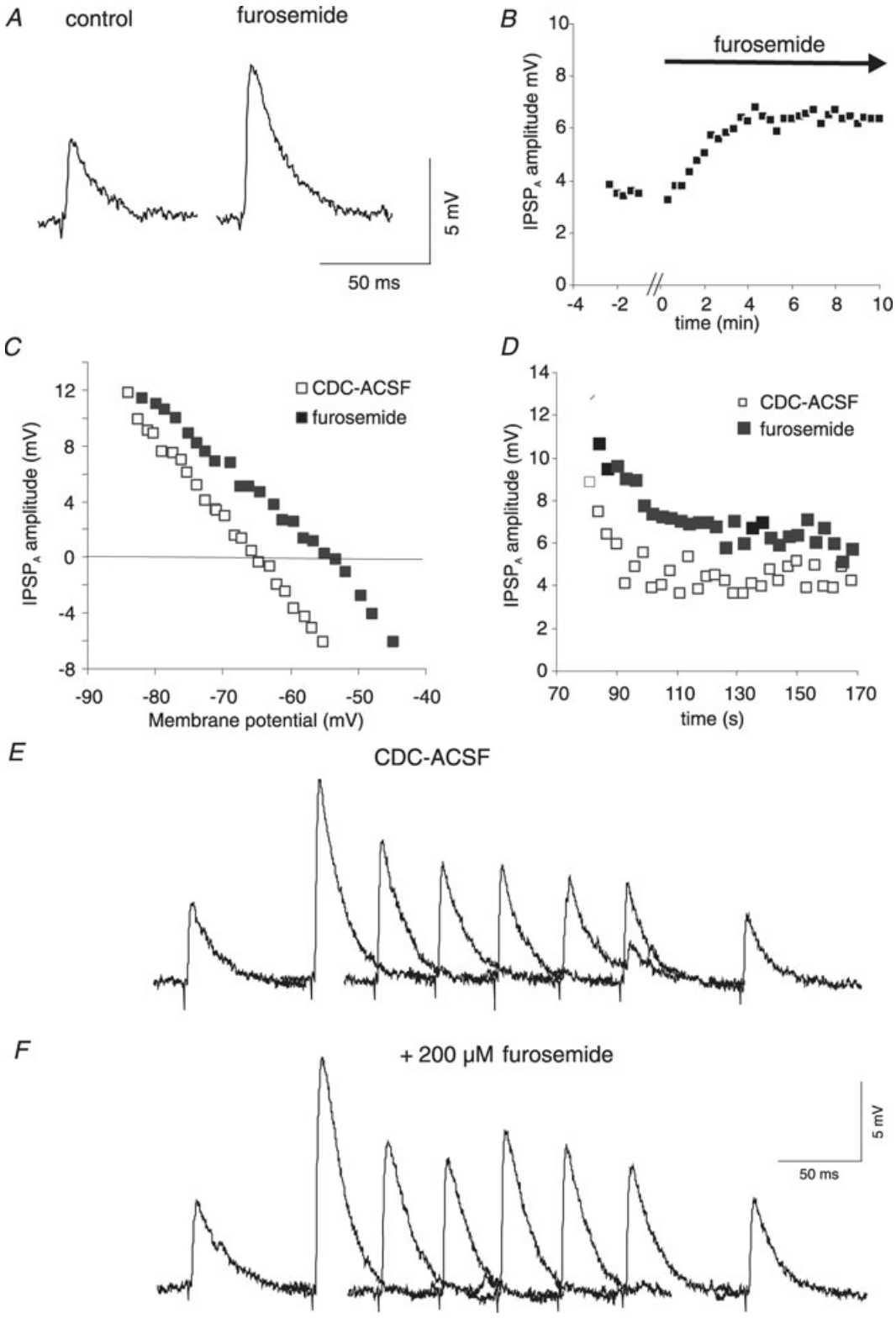

Figure 3. Effects of furosemide on rat cortical neurones
A, two traces of pharmacologically isolated $IPSP_A$ in control and in the presence of furosemide (200 μM). The approximately twofold increase in $IPSP_A$ amplitude (from 4.6 mV to 7.6 mV) in this neurone corresponds to the average increase in driving force from 7.4 ± 2.2 mV to 14.8 ± 4.8 mV. All data illustrated in this figure were obtained with KCl-filled microelectodes. *B*, plot of the average amplitude of the isolated $IPSP_A$ during the washing in of furosemide (200 μM). The gap of data points represents about 1 min, required for

Finally, we considered the participation of voltage-activated Cl^- channels in the efflux of $[Cl^-]_i$ by evaluating the effects of 9AC, a blocker of ClC2 (Clark *et al.* 1998). Application of 9AC (50 μM) had no effect on the amplitude of isolated $IPSP_A$ (control: 4.0 ± 2.3 mV; 10 min 9AC: 3.0 mV $\pm$ 1.7 mV; $n = 6$, $P > 0.5$). In the presence of 9AC, the recovery τ increased from 6.6 ± 2.7 s to 8.4 ± 4.2 s ($n = 7$; Fig. 8*A–C*; $P < 0.05$; 6 neurones in CDC-ACSF, 1 in ACSF) and returned to control values after washout (5.9 ± 1.0 s, $n = 4$). The $E_{IPSP\text{-}A}$ was unaltered by 9AC (CDC-ACSF: -60.8 ± 4.9 mV, CDC-ACSF plus 9AC: -60.5 ± 5.0 mV; $n = 6$, $P > 0.5$; see Fig. 4*E*), despite the significant slowing of recovery by 9AC (Fig. 8). The $[Cl^-]_i$ averaged 11.9 ± 1.2 mM and 11.2 ± 1.5 mM in CDC-ACSF and 9AC, respectively ($n = 5$, $P > 0.05$). Interestingly, Cl^- injection (1 nA, 1 min) increased $[Cl^-]_i$ to 16.9 ± 3.4 mM in CDC-ACSF and to 21.7 ± 9.2 mM in the presence of 9AC. Thus $[Cl^-]_i$ increased by 5.0 mM in control and by 10.5 mM in the presence of 9AC ($n = 5$; $P = 0.059$). The larger increase of $[Cl^-]_i$ by current injection might indicate that 9AC-sensitive pathways were active during current injection, impeding an effective Cl^- loading. To test whether 9AC indeed affects an unselective pathway of Cl^- extrusion, we also applied 9AC to neurones recorded with KNO_3-filled electrodes (Fig. 7*A*, *B*). Application of 9AC increased the τ of recovery from NO_3^- loading from 19.3 ± 5.2 s to 41.7 ± 8.5 s ($n = 4$, $P < 0.05$: Fig. 7*C* and *D*), indicating that 9AC reduced a relatively unselective, NO_3^--carrying pathway in cortical neurones.

Taken together, these data indicate that all of the established Cl^- pathways join forces to extrude Cl^-, yet bumetanide and 9AC have marginal effects on the steady state reversal potential.

Rates of Cl^- efflux via the various transport routes

The relative contribution of efflux pathways to the kinetics of Cl^- extrusion appears to vary, judging from the distinct increases in τ induced by the various experimental manipulations. To test this possibility, we estimated the individual rates of Cl^- efflux using eqns (1)–(5) (see Methods). The data are given in Table 1. The flux rate mediated by NKCC1 can be estimated from eqn (2) as the difference in Cl^- flux rates obtained with and without bumetanide ($0.0263\ s^{-1}$). The Cl^- flux mediated by ClC2 (eqn (3)) can be estimated as the rate difference between control and in the presence of 9AC ($0.0336\ s^{-1}$). Application of 9AC to neurones recorded with KNO_3-filled electrodes yielded a slightly smaller rate for NO_3^- ($0.0278\ s^{-1}$), indicating that ClC2 has an apparent permeability ratio for Cl^-:NO_3^- of 0.83. Assuming that AE and ClC2 represent relatively unselective pathways carrying Cl^- and NO_3^-, the flux rate mediated by the AE can be calculated from the rate of NO_3^- extrusion ($0.0475\ s^{-1}$) minus the NO_3^- rate mediated by ClC2 ($0.0278\ s^{-1}$), i.e. $0.0197\ s^{-1}$. The rate obtained from the NO_3^- extrusion, in turn, provides a rate for the more selective pathways, presumably KCC2 and NKCC1 (total rate of $0.1456\ s^{-1}$ minus the rate mediated by unselective pathways of $0.0475\ s^{-1}$), i.e. $0.0981\ s^{-1}$. Finally, the rate mediated by KCC2 can be calculated from the rate in CDC-ACSF minus the rates mediated by NKCC1 ($0.0263\ s^{-1}$), AE ($0.0197\ s^{-1}$) and ClC2 ($0.0336\ s^{-1}$), yielding $0.0659\ s^{-1}$. The reliability of these admittedly simplistic estimates will be detailed in the Discussion. Overall, we propose that the relative contribution of the pathways to the total flux in healthy cortical neurones is as follows: KCC2 45.3%, NKCC1 18.1%, AE 13.6% and ClC2 23.1%.

Cl^- extrusion in HENC neurones

With the same experimental conditions, we evaluated the kinetics of Cl^- transport in HENC neurones. Recordings with KCl-filled microelectrodes revealed only small changes in synaptic potentials following neurone impalement. In fact, the synaptic responses obtained with KCl-filled electrodes looked, at first glance, fairly similar to those obtained with KAc-filled electrodes. Determination of the apparent $E_{IPSP\text{-}A}$ yielded an average of -48.8 ± 8.1 mV in ACSF ($n = 87$) and -59.7 ± 7.8 mV in CDC-ACSF ($n = 53$, $P < 0.0001$ *vs.* ACSF), the latter value corresponding to a $[Cl^-]_i$ of 11.2 mM. The $E_{IPSP\text{-}A}$ obtained with KCl-filled electrodes in CDC-ACSF were

the furosemide-containing CDC-ACSF to reach the chamber. *C*, plot of the $IPSP_A$ amplitudes *vs.* E_m varied by incremental current injection (from -0.5 nA to $+0.6$ nA). A linear regression of the data points (not shown) revealed a shift of the $E_{IPSP\text{-}A}$ from -65.2 mV to -55.2 mV. *D*, plot of the $IPSP_A$ amplitude following cessation of current injection from the records shown in panels *E* and *F*. The exponential fit to the data points (not shown) yields 7 s in control and 13 s in the presence of furosemide. *E*, traces of the isolated $IPSP_A$ before and after current injection. The samples shown were obtained before current injection and 6, 9, 12, 15, 18, 21 and 130 s after the end of current injection. The scale of the panels *E* and *F* refers only to the individual traces. The traces have been partly superimposed. *F*, traces corresponding to those of panel *E* from the same neurone obtained in the presence of 200 μM furosemide. A bar graph summarizing these data is shown in Fig. 11*D* to facilitate comparison with the data obtained in HENC neurones.

similar to those obtained with KAc-filled electrodes ($P > 0.05$). Resting E_m was, on average, indistinguishable between the two recording conditions and solutions (~ -71 mV).

In ACSF, the injection of Cl^- caused a further increase in the apparent $IPSP_A$ amplitude (near 15 ms post-stimulus), which slowly returned to the preceding control value. The recovery τ following injections of different amounts of Cl^- was similar, small and large Cl^- loads (e.g. 1 nA, 30 s *vs.* 2 nA 1 min) yielded τ values of 17.9 ± 10.2 s ($n = 11$) and 19.4 ± 9.2 s, respectively ($n = 22$; $P > 0.05$). Therefore, the values of different injections were averaged for each neurone, and on average a τ of 20.3 ± 11.4 s ($n = 85$) was obtained. The recovery τ exhibited a marked variability in a given tissue. Both fast recoveries (<11.5 s, mean τ of rat neurones +2 S.D.) and slow recoveries (>11.5 s) were obtained in 14 of 29 resections with more than one recorded neurone in control conditions. The variability of recovery τ values persisted in the presence of CDC-ACSF (see Fig. 9*A*) and on average the $IPSP_A$ recovered with a tau of 19.0 ± 9.6 s ($n = 62$, $P > 0.5$ *vs.* ACSF). It should be pointed out that the mean τ of

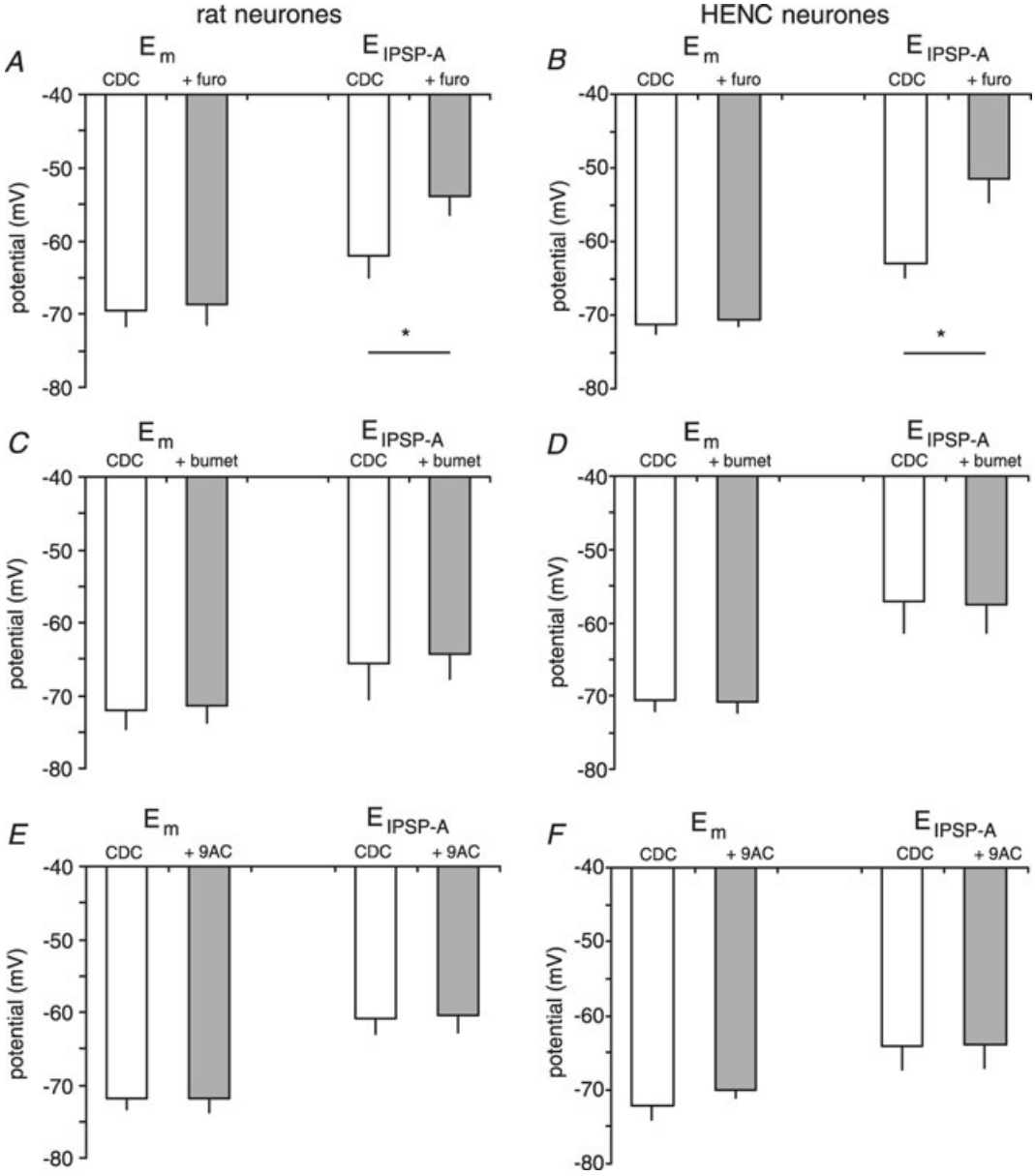

Figure 4. Effects of various antagonists on E_m and E_{IPSP-A} in rat and HENC neurones
Plot of E_m and E_{IPSP-A} obtained with KCl-filled microelectrodes in CDC-ACSF-containing furosemide (furo), bumetanide (bumet) or 9AC as indicated. Panels *A*, *C* and *E* summarize the effects of antagonists on E_m and E_{IPSP-A} in rat neocortical neurones as indicated. Panels *B*, *D* and *F* summarize the effects of antagonists on E_m and E_{IPSP-A} in HENC neurones as indicated.

all rat neurones was 7.2 ± 2.4 s in CDC-ACSF, and only three neurones exhibited τ values larger than 11.5 s (i.e. outliers above the mean +2 S.D.). In the human tissues only 12 of 62 neurones were below this border (average 9.3 ± 1.8 s), i.e. the majority of neurones exhibited a considerably slower Cl^- extrusion (average 21.4 ± 9.3 s, $n = 50$; $P < 0.0001$). To test whether this large scatter of data represents statistically significant deviation from a normal distribution we used the Kolmogorov–Smirnov test with Lilliefors's significance correction and the Shapiro–Wilk test, both indicating significant differences ($P = 0.038$ and $P = 0.000$, respectively).

To test whether the variability of tau values relates to the dichotomy of $E_{IPSP\text{-}A}$ in HENC neurones, we compared the reversal potentials of neurones with relatively small and large time constants. To this end, the reversal potentials of 48 neurones were segregated into two groups according to the above border of τ (11.5 s). Neurones

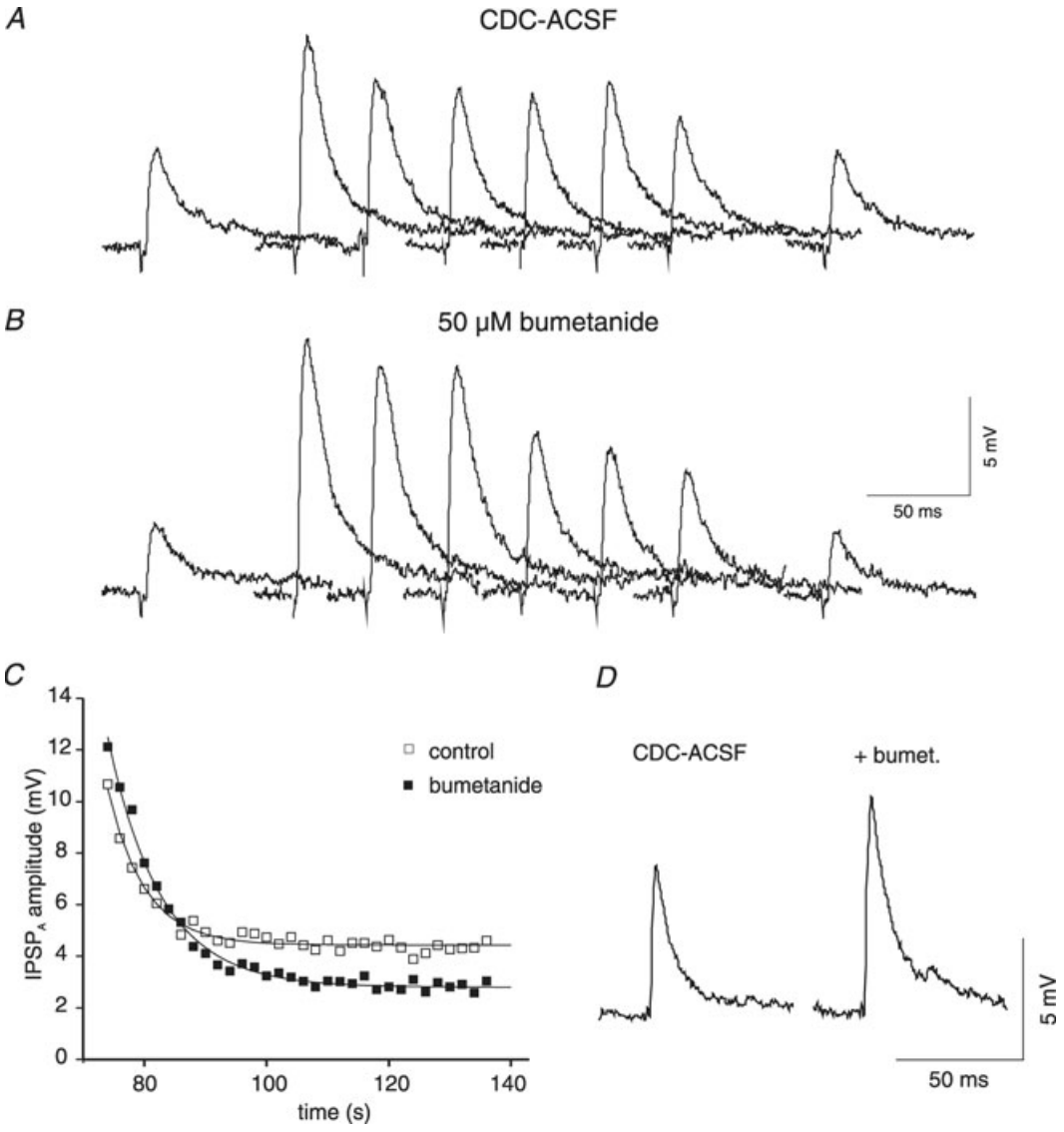

Figure 5. Effects of bumetanide on rat neurones
A, traces of isolated $IPSP_A$ before and after current injection from a KCl-filled microelectrode. The samples shown were obtained in CDC-ACSF before current injection and 0, 2, 4, 6, 8, 10 and 60 s after the end of current injection (2 nA, 1 min). *B*, traces from the same neurone as shown in *A* in the presence of 50 μM bumetanide corresponding to traces shown in panel *A*. *C*, plot of the $IPSP_A$ amplitude following cessation of current injection in CDC-ACSF (open squares) and after addition of 50 μM bumetanide (filled squares). The symbols represent the average values of three consecutive injections. The curves represent a single exponential fit with tau values of 6.0 s (CDC-ACSF) and 8.7 s (bumetanide). The average time constants have been plotted together with data from HENC neurones (see Fig. 10*D*). *D*, traces of the isolated $IPSP_A$ from a rat cortical neurone in CDC-ACSF and after 10 min of bumetanide application.

with time constants below this border had an average τ of 9.3 ± 1.9 s ($n = 11$) and a mean $E_{\text{IPSP-A}}$ of -64.1 ± 4.5 mV ($n = 11$), indistinguishable from rat neurones recorded with KCl electrodes ($P > 0.05$). The remaining neurones clearly had a larger τ (19.5 ± 6.0 s) and exhibited a less negative $E_{\text{IPSP-A}}$ (average -58.9 ± 7.5 mV; $n = 37$, $P < 0.05$ *vs.* neurones with small τ), as was obvious from the approximately linear relation (see Fig. 9*B*). This indicates that less negative reversal potentials and increases in the depolarizing driving force of IPSP_A are related to the large tau (Fig. 9*C*).

In CDC-ACSF, we calculated the changes in $E_{\text{IPSP-A}}$ and $[\text{Cl}^-]_\text{i}$ induced by current injections (see Methods). Applying 1 nA for 1 min increased $[\text{Cl}^-]_\text{i}$ from 11.8 ± 4.5 mM to 19.8 ± 8.3 mM ($n = 23$, $P < 0.0001$) after current injection, i.e. by 7.9 ± 4.5 mM. This is a significantly larger increase than under the same conditions in rat neurones ($P < 0.01$). In a subset of these

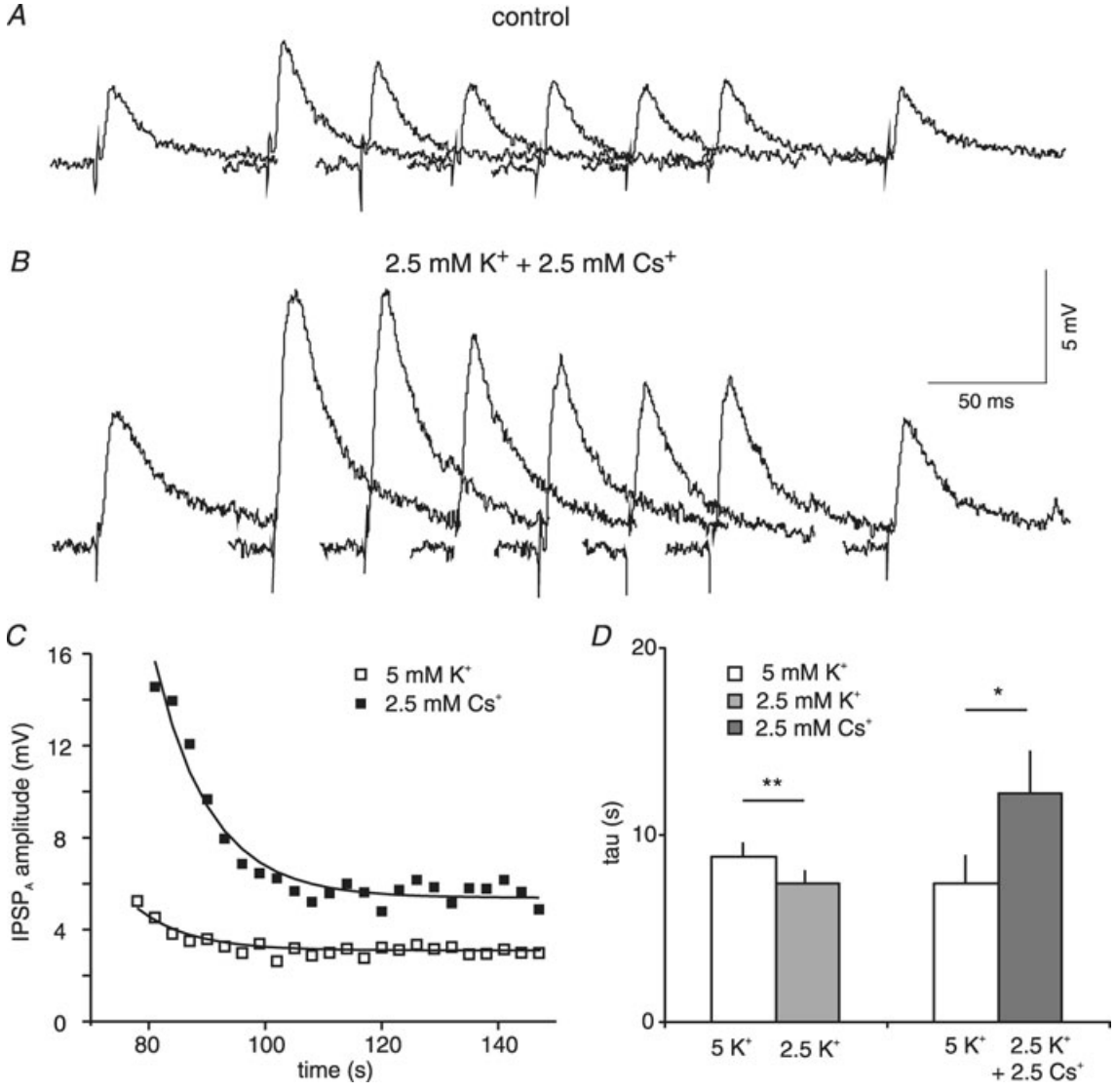

Figure 6. Effects of Cs^+ on IPSP_A recovery in rat neurones
A, traces of isolated IPSP_A before and after current injection from a KCl-filled microelectrode. The samples shown were obtained in 5 mM K^+ CDC-ACSF before current injection and 6, 9, 12, 15, 18, 21 and 130 s after the end of current injection. *B*, traces from the same neurone as shown in *A* in the presence of 2.5 mM K^+ and 2.5 mM Cs^+ CDC-ACSF corresponding to the traces shown in panel *A*. The scale in panel *B* refers only to the individual traces in panels *A* and *B*. Traces have been partly superimposed. *C*, plot of the average IPSP_A amplitude following cessation of current injection from the recordings shown in panel *A* and *B*. The exponential fit to the data points yields a tau of 6.1 s in 5 mM K^+ CDC-ACSF (open symbols) and 9.5 s in the presence of 2.5 mM K^+ and 2.5 mM Cs^+ (filled symbols). *D*, plot of the mean IPSP_A time course on reducing $[K^+]_\text{o}$ from 5 mM to 2.5 mM and replacing 2.5 mM K^+ with 2.5 mM Cs^+ as indicated.

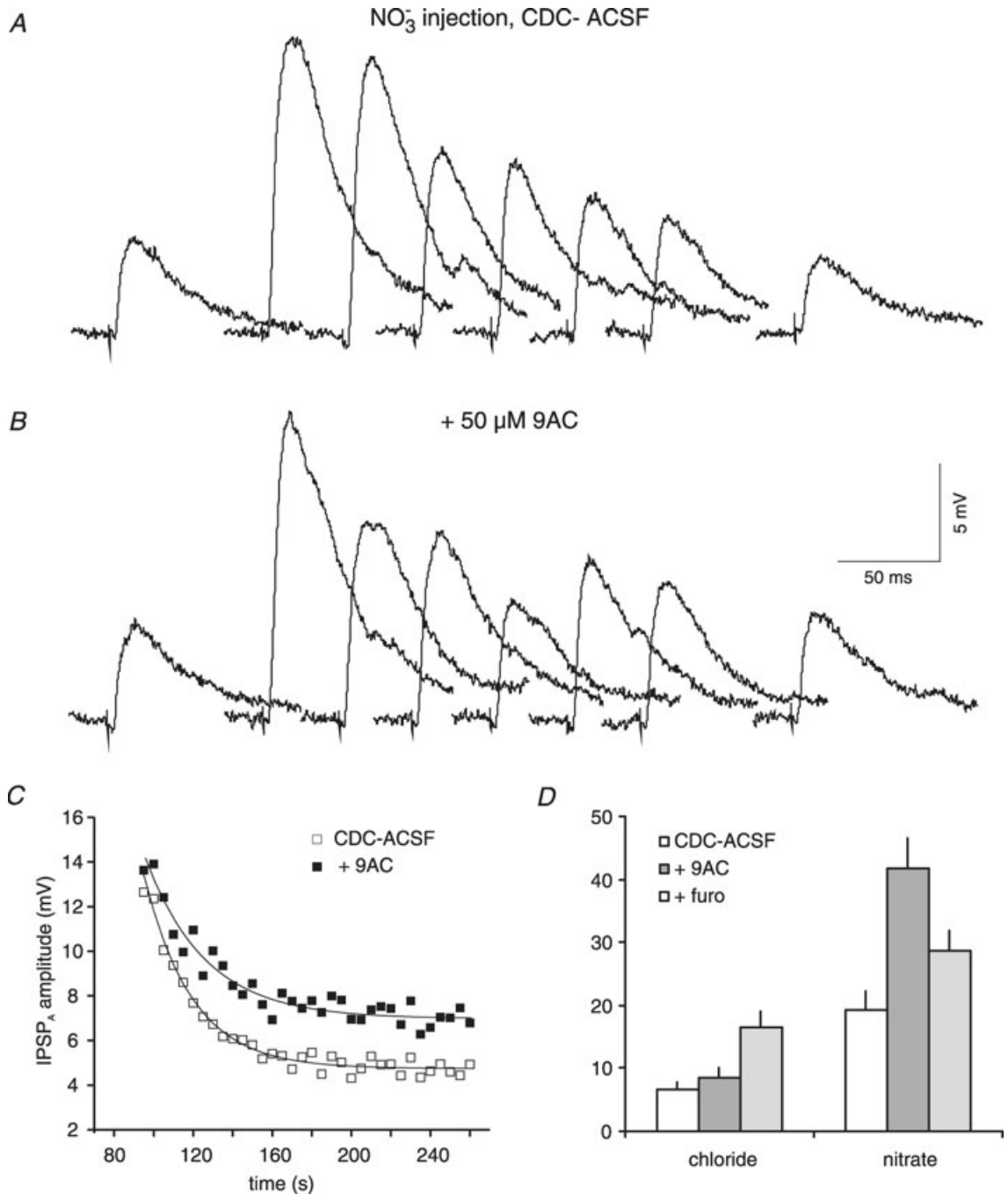

Figure 7. Effects of NO_3^- injection into rat neurones
A, traces of isolated $IPSP_A$ before and after NO_3^- injection. The samples shown were obtained in CDC-ACSF before current injection and 0, 10, 20, 30, 40, 50 and 300 s after the end of current injection (1 nA, 1 min). *B*, traces from the same neurone as shown in *A* in the presence of 50 μM 9AC, corresponding to traces shown in panel *A*. *C*, plot of the $IPSP_A$ amplitude following cessation of current injection in CDC-ACSF (open squares) and after addition of 50 μM 9AC (filled squares). The symbols represent the average values of three consecutive injections. The curves represent single exponential fits to the data with tau values of 24.1 s (CDC-ACSF) and 30.3 s (9AC). *D*, plot of the mean τ values following Cl^- and NO_3^- injections in CDC-ACSF (open columns), in the presence of 50 μM 9AC (dark grey columns) and in the presence of 200 μM furosemide (light grey columns). The CDC-ACSF values given are from the 9AC series of measurements.

neurones (E_m: -71.3 ± 2.1 mV, $E_{IPSP\text{-}A}$: -57.6 ± 7.3 mV), we compared the effects of different current injection magnitudes. Injection of 1 nA for 1 min shifted $E_{IPSP\text{-}A}$ to -45.3 ± 9.3 mV, indicating an increase of $[Cl^-]_i$ to 22.8 ± 9.3 mM ($n = 6$, $P < 0.05$ *vs.* baseline for both). Injection of 2 nA for 1 min shifted $E_{IPSP\text{-}A}$ to -36.4 ± 14.7 mV, indicating an increase of $[Cl^-]_i$ to 35.7 ± 18.8 mM ($n = 6$, $P < 0.05$ *vs.* baseline for both). The estimated peak $E_{IPSP\text{-}A}$ and $[Cl^-]_i$ induced by the two current magnitudes were significantly different from steady state values and from each other ($P < 0.05$). The increase of $[Cl^-]_i$ over baseline (1 nA: by 9.8 ± 5.1 mM, 2 nA: by 23.7 ± 16.9 mM) was about twofold larger on doubling the current ($P < 0.05$).

Pharmacology of Cl^- transport in HENC neurones

We first considered the possibility that an up-regulated NKCC1 (Palma *et al.* 2006) might cause an augmented inward transport in HENC neurones, as occurs perinatally (Dzhala *et al.* 2005). Application of bumetanide had no consistent effect on the amplitude of the pharmacologically isolated $IPSP_A$ (CDC-ACSF: 5.0 ± 3.2 mV; bumetanide: 6.4 ± 3.9 mV; $n = 9$, $P > 0.05$). The $E_{IPSP\text{-}A}$ was unaffected by bumetanide (CDC-ACSF: -57.2 ± 9.4 mV, bumetanide: -57.6 ± 8.5 mV; $n = 6$; $P > 0.05$; see Fig. 4*D*), and hence $[Cl^-]_i$ was unaltered at 12.5 and 12.2 mM, respectively. Repeating Cl^- injections during application of bumetanide (10 μM, $n = 3$; or

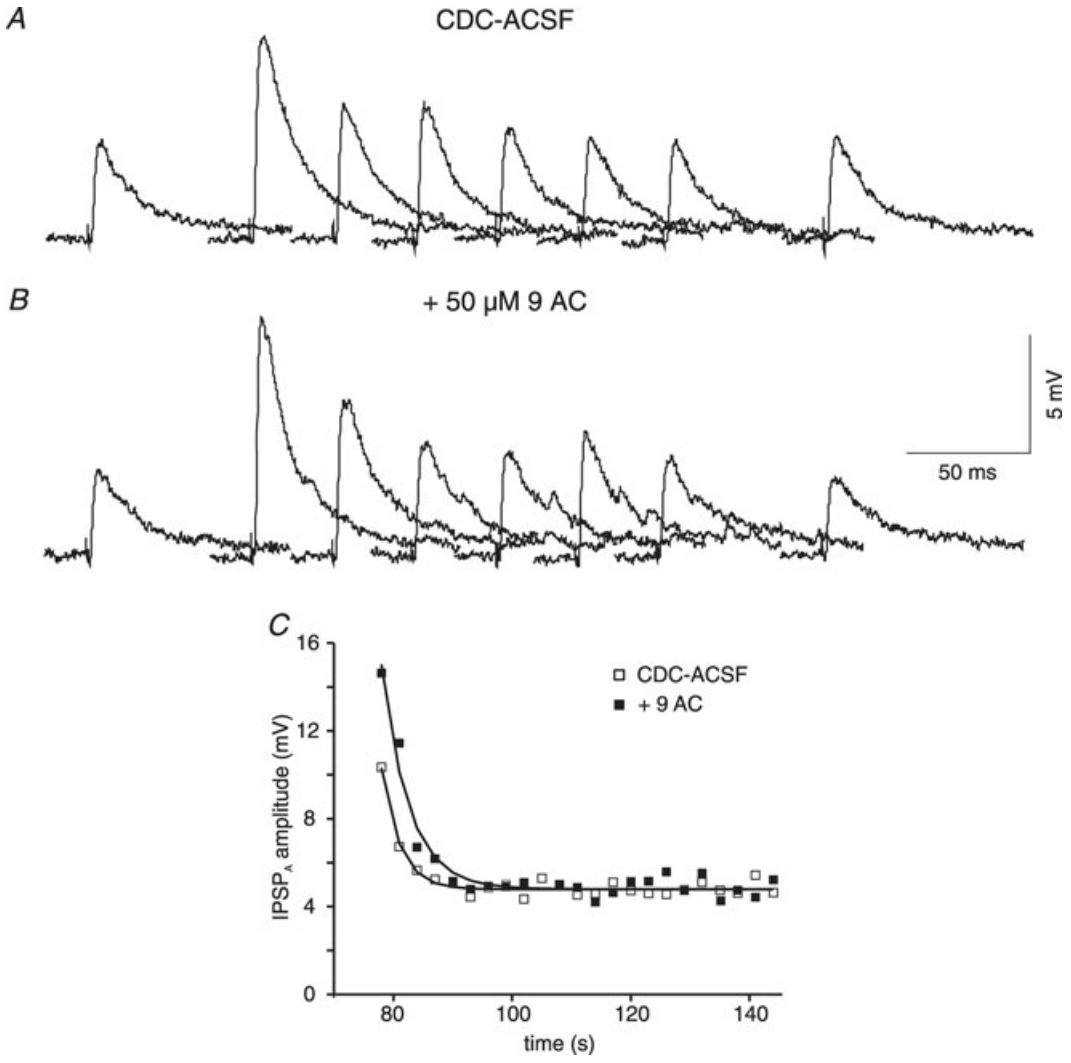

Figure 8. Effects of 9AC on rat cortical neurones
A, traces of isolated $IPSP_A$ before and after Cl^- injection. The samples shown were obtained in CDC-ACSF before current injection and 0, 3, 6, 9, 8, 12 and 60 s after the end of current injection (1 nA, 1 min). *B*, traces from the same neurone as shown in *A* in the presence of 50 μM 9AC, corresponding to the traces shown in panel *A*. *C*, plot of the $IPSP_A$ amplitude following cessation of Cl^- injection in CDC-ACSF (open squares) and after addition of 50 μM 9AC (filled squares). The symbols represent the average values of three consecutive injections. The curves represent a single exponential fit with time constants of 3.1 s (CDC-ACSF) and 4.6 s (9AC).

Table 1. Time constants of recovery of rat neurones under the different experimental condition

Condition	τ (s)	Rate (s^{-1})	Isol. rates (s^{-1})	Calculation of rates for the different pathways			
ACSF	7.85 ± 2.41(84)	0.1273					
CDC-ACSF	6.87 ± 2.36(44)	0.1456					0.1456
CDC-ACSF	7.01 ± 1.67(12)	0.1426					
With bumet.	8.60 ± 1.61(12)	0.1163	0.0263	0.0263			−0.0263
CDC-ACSF	7.12 ± 2.97(8)	0.1405					
With furosemide	16.57 ± 6.69(8)	0.0603	0.0801				
CDC-ACSF	6.58 ± 2.72(7)	0.1521					
With 9AC	8.44 ± 4.16(7)	0.1185	0.0336		0.0336		−0.0336
CDC-5 mM K^+	7.13 ± 2.95(5)	0.1402					
CDC-2.5 mM Cs^+	12.23 ± 4.45(5)	0.0818	0.0584				
CDC/nitrate	21.06 ± 6.06(17)	0.0475	0.0475			0.0475	
With furosemide	28.60 ± 4.56(3)	0.0350					
CDC/nitrate	19.32 ± 5.22(4)	0.0518					
With 9AC	41.68 ± 8.49(4)	0.0240	0.0278			−0.0278	−0.0197
			rate:	0.0263	0.0336	0.0197	0.0659
			pathway:	NKCC1	ClC2	AE	KCC2

The time constants in control CDC-ACSF differ in some of the subgroups from the ensemble average. The rates were therefore calculated for each experimental group as difference in rate with and without the drugs. On the right hand the calculation of the rates of the individual pathways is presented. From the different rates obtained with 9AC for Cl^- and NO_3^- extrusions, a relative permeability of ClC2 of Cl^- *vs.* NO_3^- was calculated (0.83). Note that three neurones were not included in the average of the CDC-ACSF group, because the values were considered outliers (above the mean +2 S.D.).

50 μM, $n = 5$) in CDC-ACSF revealed a consistent increase in the recovery τ from 19.4 ± 4.5 s to 24.0 ± 3.2 s ($n = 8$, $P < 0.05$; Fig. 10*A–C*). In some neurones we calculated the maximal $[Cl^-]_i$ attained after injection, suggesting a $[Cl^-]_i$ of 22.1 ± 11.9 mM in control and 19.9 ± 7.6 mM in bumetanide ($n = 5$, $P > 0.05$), and hence $[Cl^-]_i$ increased by 7.4 and 6.8 mM, respectively. On return to CDC-ACSF, the τ recovered to control values (17.5 ± 2.4 s, $n = 4$; $P < 0.05$ *vs.* bumetanide, $P > 0.05$ *vs.* control). These data indicate that bumetanide has, on average, no effect on the $E_{IPSP\text{-}A}$ (Fig. 4*D*) despite a marked prolongation of recovery τ after Cl^- loading (Fig. 10*D*).

Application of furosemide (200 μM) markedly increased the amplitude of isolated $IPSP_A$ from 5.0 ± 2.4 mV to 9.0 ± 4.2 mV ($n = 8$, $P < 0.001$). Comparison of the $E_{IPSP\text{-}A}$ before and during the presence of furosemide revealed a marked shift from −61.1 ± 4.0 mV to −49.4 ± 5.4 mV ($n = 6$, $P < 0.05$, see Fig. 4*B*), corresponding to an increase in $[Cl^-]_i$ from 10.5 ± 1.9 mM to 18.3 ± 4.5 mM ($n = 6$, $P < 0.05$). Furosemide also caused a marked increase in the τ of recovery from Cl^- loading in HENC neurones. In three neurones, application of furosemide in ACSF increased the recovery τ from 20.4 ± 4.2 s to 50.0 ± 22.0 s. Application of furosemide in CDC-ACSF increased the τ from 15.5 ± 6.0 s to 44.1 ± 11.4 s ($n = 8$, $P < 0.001$; Fig. 11*C*, *D*). The maximal $[Cl^-]_i$ reached after cessation of current injection was 18.7 ± 2.4 mM in CDC-ACSF and 26.9 ± 5.0 mM in the presence of furosemide ($n = 6$, $P < 0.01$). The actual increase of $[Cl^-]_i$ by Cl^- injection was unaltered (CDC-ACSF: 8.3 ± 1.8 mM; furosemide: 8.7 ± 5.4 mM; $n = 6$, $P > 0.05$). On return to CDC-ACSF, the τ recovered to the preceding control value (14.1 ± 6.4 s; $n = 6$, $P < 0.001$ *vs.* furosemide and $P > 0.5$ *vs.* CDC-ACSF). The $E_{IPSP\text{-}A}$ also essentially recovered to control values (−66.3 ± 6.4 mV; $n = 4$, $P < 0.01$ *vs.* furosemide, $P > 0.05$ *vs.* preceding control).

At this stage, the pharmacological evaluation had not revealed much about the underlying deficits of Cl^- outward transport in most of the HENC neurones. To delineate the underlying deficits, changes in $[K^+]_o$ were carried out. Reducing $[K^+]_o$ from 5 to 2.5 mM had no significant effect on the kinetics of Cl^- extrusion. In 2.5 mM K^+, the τ of recovery was 17.5 ± 5.5 s compared with 16.8 ± 6.2 s under control conditions (5 mM K^+ CDC-ACSF; $n = 11$, $P > 0.05$, Fig. 12*D*). The $E_{IPSP\text{-}A}$ increased from −60.8 ± 6.6 mV to −67.2 ± 8.1 mV in the presence of 2.5 mM K^+ ($n = 7$, $P < 0.05$), exceeding the shift in E_m (from −70.8 ± 3.9 mV to −73.2 ± 4.6 mV, $P < 0.05$).

A deficit of K^+-dependent routes of Cl^- extrusion was further tested by equimolar replacement of 2.5 mM K^+ with Cs^+. The τ increased slightly from 15.0 ± 4.7 s (CDC-ACSF with 5 mM K^+) to 17.5 ± 6.0 s (CDC-ACSF with 2.5 mM K^+ and 2.5 mM Cs^+; $n = 9$; $P < 0.05$; Fig. 12*A* and *B*). Comparison of the $E_{IPSP\text{-}A}$ revealed no effect of Cs^+ (−61.9 ± 6.3 mV in CDC-ACSF and −60.3 ± 4.2 mV in the presence of 2.5 mM Cs^+; $n = 8$, $P > 0.05$). These data suggest that the kinetics of Cl^- extrusion from

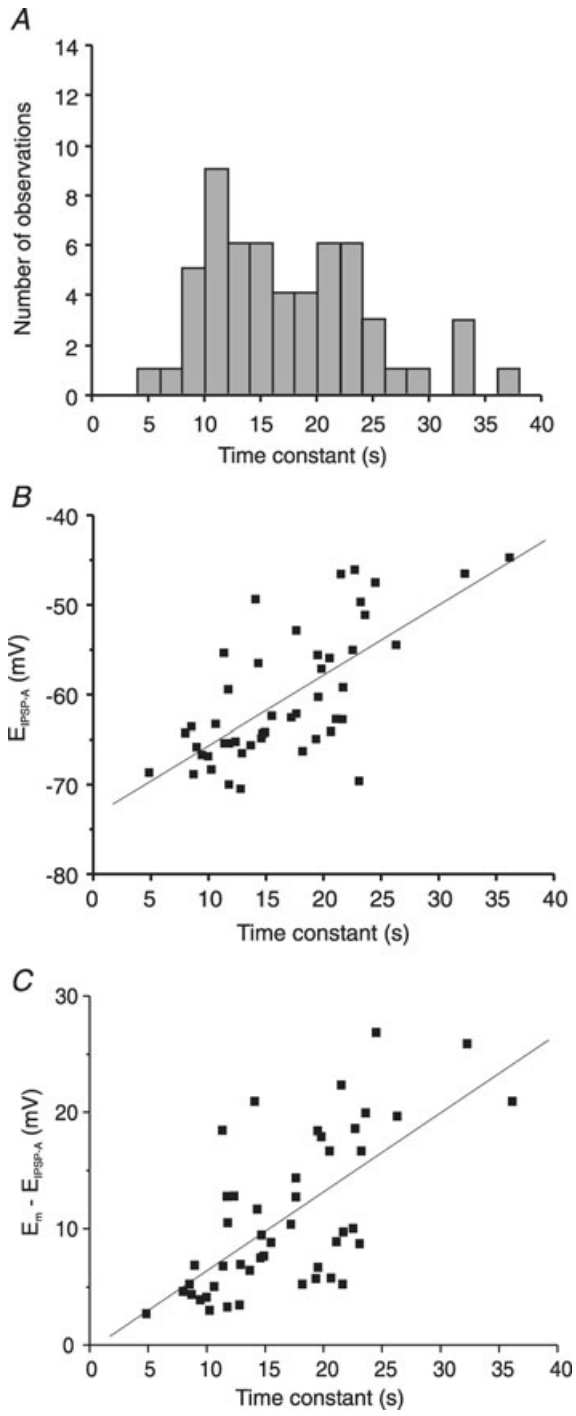

Figure 9. Parameters of inhibition in HENC neurones
A, histogram of $IPSP_A$ recovery time constant of HENC neurones. Three neurones with time constants exceeding 40 s (42.4 s, 48.0 s and 54.3 s) are not shown in the graph to maintain the scaling of Fig. 2*E*. The plot reveals that 16 neurones had τ values <12 s, 20 neurones had τ values between 12 and 20 s, and the τ of 24 neurones was >20 s. *B*, plot of the E_{IPSP-A} *vs.* the τ of $IPSP_A$ recovery following Cl^- injection. *C*, plot of the driving force (E_m – E_{IPSP}) of neurones from HENC neurones recorded with KCl-filled microelectrodes *vs.* the time constant of $IPSP_A$ recovery.

HENC neurones exhibits no detectable K^+ and low Cs^+ sensitivity (see Fig. 12*D*). Thus the large τ recovery in HENC neurones may relate to a deficit of K^+-dependent pathways, i.e. KCC2.

The contribution of other routes of Cl^- extrusion was investigated by iontophoresis of NO_3^-. Unfortunately, recording with KNO_3-filled electrodes was difficult in HENC neurones. Impaled neurones were more fragile and in some, spontaneous synaptic activity at high frequency and large amplitude prevented determination of the τ of recovery in ACSF. Nevertheless, recovery from NO_3^- loading was observed in CDC-ACSF at a mean τ of 35.5 ± 17.3 s ($n = 7$). This is much larger than the τ of recovery from Cl^- loading ($P < 0.001$, Fig. 13*C*). Recovery from NO_3^- injections in HENC neurones was also considerably slower than in rat cortical neurones ($P < 0.01$). This suggests that not only the fairly selective routes of Cl^- extrusion (KCC2, NKCC1), but also the unselective, i.e. NO_3^--carrying, pathways (AE and/or ClC2) may be impaired in HENC neurones.

To test which of the two presumed unselective pathways, AE or ClC2, was reduced we applied 9AC. 9AC (50 μM) had no consistent effect on E_m (see Fig. 4*F*) or the amplitude of the pharmacologically isolated $IPSP_A$ (control: 3.3 ± 3.2 mV, 9AC: 3.3 ± 2.7 mV; $n = 7$, $P > 0.5$). Accordingly, E_{IPSP-A} and $[Cl^-]_i$ were unaltered by 9AC (CDC-ACSF: -63.2 ± 6.7 mV, 9.6 ± 3.2 mM; 9AC: -62.3 ± 5.5 mV, 10.0 ± 3.0 mM; $n = 8$, $P > 0.05$ for both pairs). The recovery τ of the isolated $IPSP_A$ was marginally increased, from a mean 14.2 ± 6.2 s in CDC-ACSF to 16.2 ± 5.2 s in CDC-ACSF containing 9AC ($n = 8$, $P < 0.05$; Fig. 14*A*–*C*). Neither the maximal $[Cl^-]_i$ at the end of Cl^- injection (control: 14.8 ± 7.0 mM; 9AC: 16.3 ± 9.1 mM; $n = 6$, $P > 0.5$) nor the increase of $[Cl^-]_i$ induced by injection of 1 nA for 1 min (control: by 5.2 ± 5.0 mM; 9AC: 6.2 ± 6.4 mM) was affected ($P > 0.05$). Compared to the considerable slowing of recovery by 9AC in rat neurones (from 6.6 to 8.4 s), the slight increase in τ suggests that 9AC-sensitive Cl^- extrusion is relatively small in HENC neurones. This view is also supported by the similar increases of $[Cl^-]_i$ in HENC neurones with and without 9AC, whereas in rat neurones the identical Cl^- load caused a twofold larger increase of $[Cl^-]_i$ in the presence of 9AC.

Rates of Cl^- efflux from HENC neurones

The time constants obtained under the various experimental conditions (Table 2) were converted into rates as described for rat neurones. The average τ obtained in CDC-ACSF yielded a total Cl^- flux rate of 0.0526 s^{-1}, 63.9% smaller than in rat neurones. From the bumetanide effects, a flux rate via NKCC1 of 0.0101 s^{-1}, was obtained,

i.e. 61.7% smaller than in rat neurones. The Cl^- flux rate via ClC2 amounted to 0.0068 s^{-1}, 79.9% smaller than in rat neurones (Fig. 15*A*). Assuming similar properties of ClC2 (i.e. only decreases in the number of transporters) the NO_3^- rate of ClC2 (0.0059 s^{-1}) was calculated using the relative permeability determined in rat neurones (0.83). Thus the flux rate provided by the AE amounted to 0.0226 s^{-1}, about 14% larger than in rat neurones.

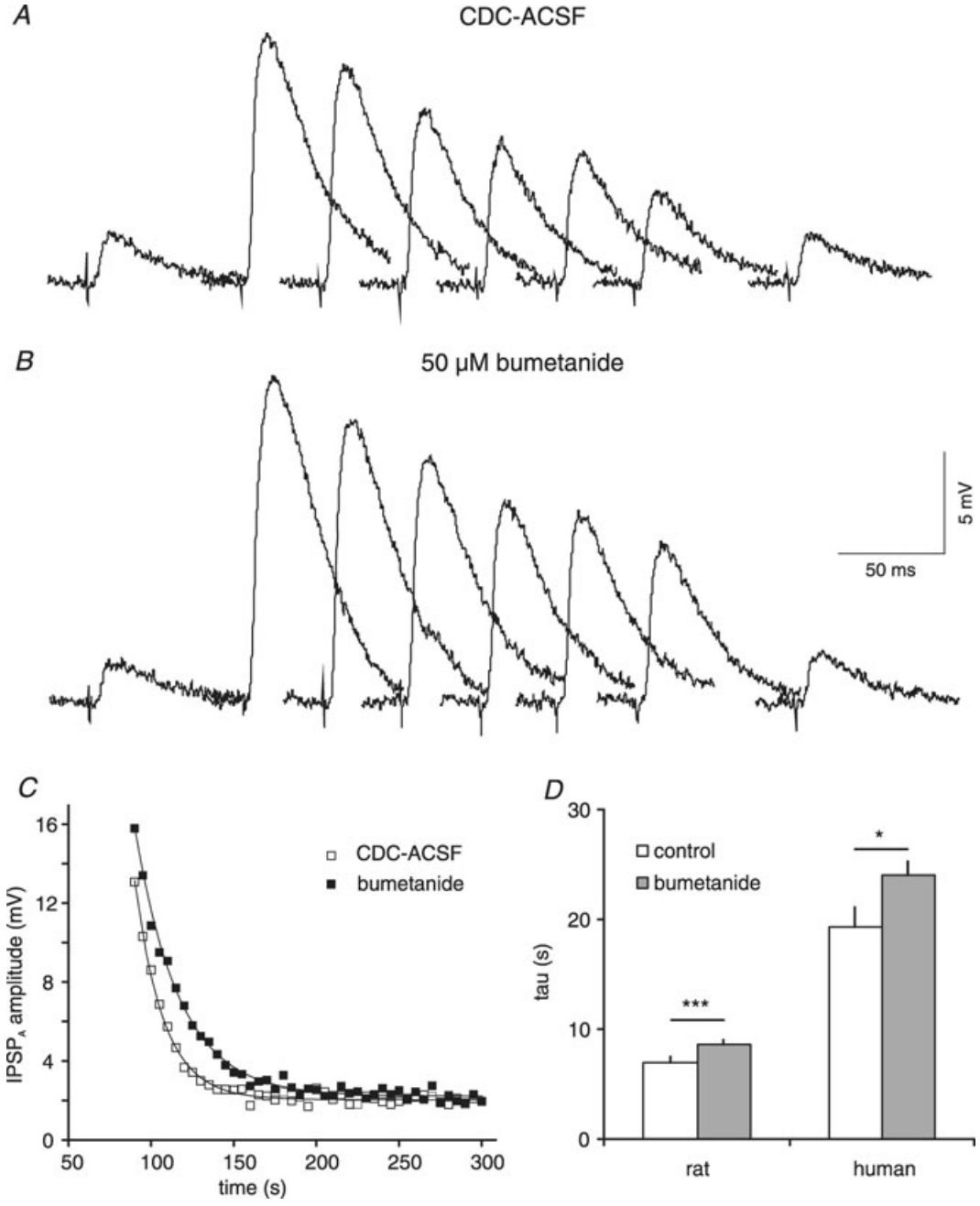

Figure 10. Effects of bumetanide on HENC neurones
A, sample traces of isolated $IPSP_A$ before and after Cl^- injection. The traces shown were obtained in CDC-ACSF before current injection and 0, 5, 10, 15, 20, 25 and 150 s after the end of current injection (2 nA, 1 min). *B*, sample traces from the same neurone as shown in *A* in the presence of 50 μM bumetanide corresponding to traces shown in *A*. *C*, plot of the $IPSP_A$ amplitude following cessation of Cl^- injection in CDC-ACSF (open squares) and during addition of 50 μM bumetanide (filled squares). The symbols represent the average of three consecutive injections. The curves represent single exponential fits with time constants of 17.4 s (CDC-ACSF) and 26.4 s (bumetanide). *D*, mean τ values in CDC-ACSF and after addition of bumetanide in rat and HENC neurones. Bumetanide was applied at both 10 and 50 μM but its effect was not increased at the higher concentration and therefore the data have been pooled.

Finally, the calculated flux rate of KCC2 was 0.0132 s^{-1} or 0093 s^{-1} from the Cs^+ experiments, i.e. 80.0% (calculated; or 84.1% from Cs^+ experiments) smaller than in rat neurones. The relative contribution of the four pathways in HENC neurones can be ranked in descending order: AE: 43.0%, KCC2: 25.0%, NKCC1: 19.2%, and ClC2: 12.9%.

The average values discussed above do not reflect possible changes in the transporters of individual neurones over time. Considering that the large scatter in time constants (Fig. 9*A*) may reflect snapshots of a progressive decline of Cl^- homeostasis, it is tempting to sort these pictures into a sequential order. First, we tested our hypothesis that a decrease in KCC2 is the crucial initial step for altered Cl^- homeostasis. In fact, changes in KCC2 mRNA and protein levels are preceded by functional reductions in KCC2 via tyrosine phosphorylation in hippocampal neurones (Wake *et al.* 2007). Therefore, we calculated the Cs^+-sensitive rate as an index for KCC2 function of individual neurones. In rat neurones, an

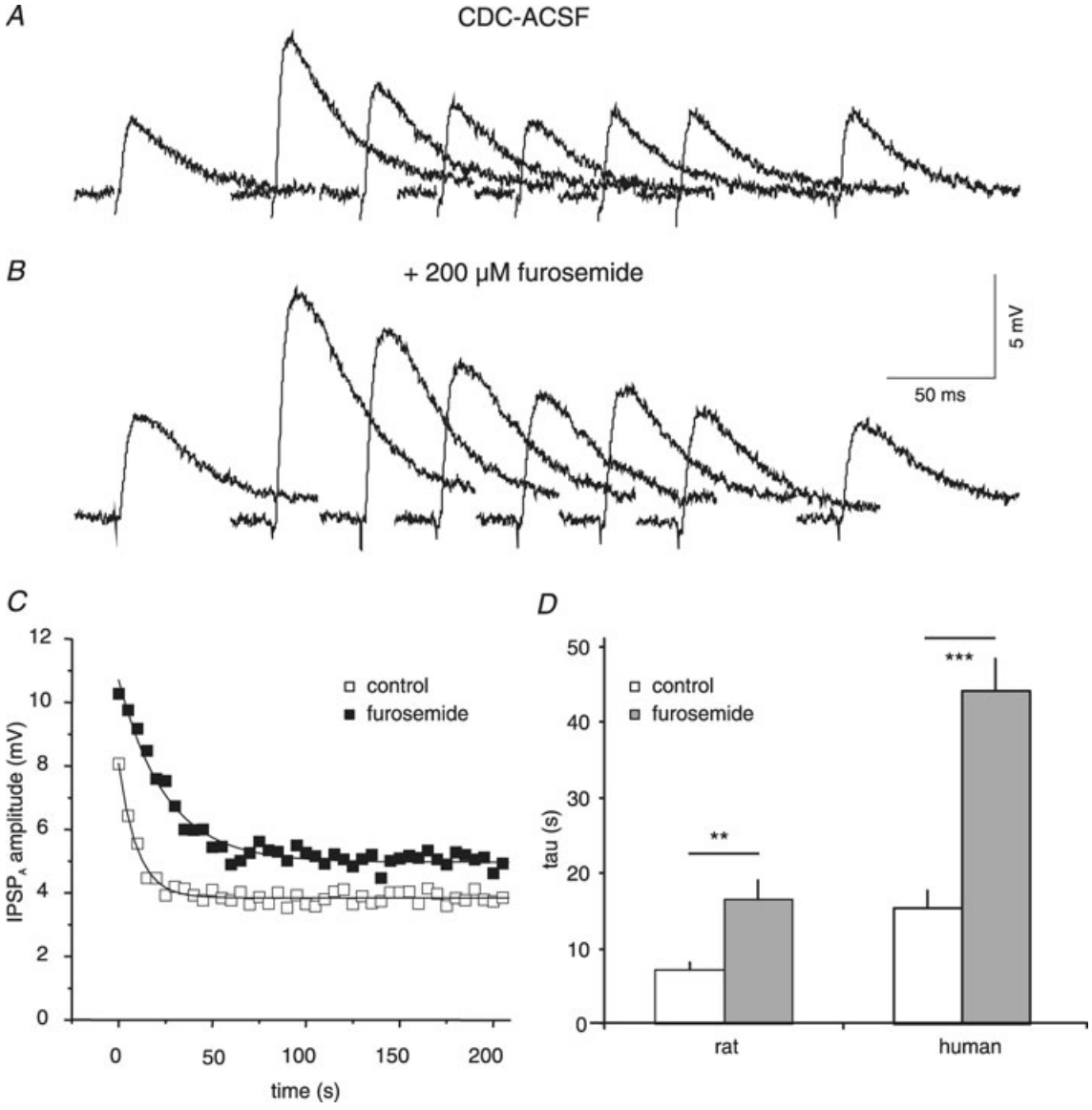

Figure 11. Effects of furosemide on the τ of $IPSP_A$ recovery in HENC neurones
A and *B*, traces of $IPSP_A$ in a HENC neurone in CDC-ACSF (*A*) and in the presence of 200 μM furosemide (*B*). The time scale refers to both sets of traces. The traces before and at 0, 10, 20, 30, 40, 50 and 260 s after the end of Cl^- injection have been partly superimposed. *C*, plot of the average $IPSP_A$ amplitude from three consecutive injections in CDC-ACSF (open squares) and CDC-ACSF plus 200 μM furosemide (filled squares). The curves drawn represent the exponential fits to the data points with τ values of 9.7 s and 25.0 s, respectively. *D*, the mean τ in rat and HENC neurones in CDC-ACSF and in the presence of 200 μM furosemide in CDC-ACSF.

average Cs^+-sensitive rate of 0.0584 s^{-1} was obtained. In HENC neurones, the rate was on average about 6-fold smaller (0.0093 s^{-1}). If KCC2 declines first, neurones with a relatively small τ should have a sizeable Cs^+-sensitive rate, and neurones with large τ values should have small rates. Segregating the neurones into two groups with τ values below or above 12 s revealed two distinct groups with mean τ values of 11.0 s and 18.3 s, respectively. The neurones with τ of 11 s exhibited a Cs^+-sensitive rate of 0.0115 ± 0.0030 s^{-1} ($n = 4$), 17% of that in rat neurones. The other group with a mean τ of 18.3 s had an even smaller value (0.0023 ± 0.0023 s^{-1}, $n = 5$, $P < 0.05$), i.e. the Cs^+-sensitive rate was 3% of that in rat neurones. This indicates that the HENC neurones with the fastest Cl^- recovery already had an 83% decrease in KCC2 function (or number of transporters) and neurones with large τ

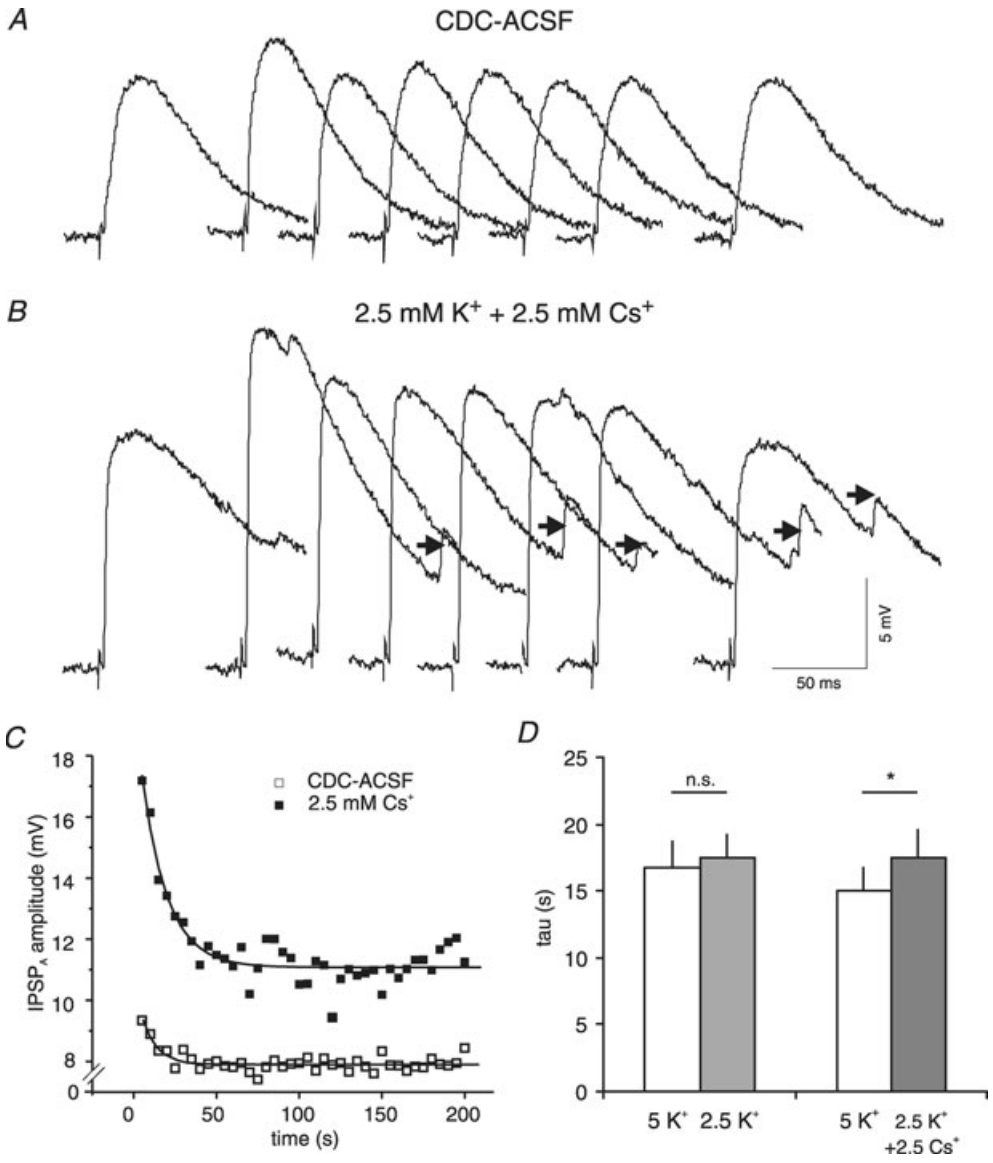

Figure 12. Effects of Cs^+ on $IPSP_A$ recovery τ in HENC neurones
A, traces of $IPSP_A$ before and 5, 10, 15, 20, 25, 30 and 90 s after Cl^- injection (1 nA, 1 min) in a HENC neurone in CDC-ACSF. *B*, traces of the same neurone in CDC-ACSF with half of $[K^+]_o$ replaced by Cs^+ before and 0, 5, 10, 15, 20, 25 and 90 s after the end of Cl^- injection (1 nA, 1 min). Note the small spontaneous $IPSP_A$ (arrows). *C*, plot of the average $IPSP_A$ amplitude after cessation of Cl^- injection in CDC-ASCF (open squares) and in the presence of Cs^+ (filled squares) from the experiment shown in *A* and *B*. The curves represent exponential fits to the data (control: 10.3 s; Cs^+: 15.4 s). *D*, plot of the mean τ values of $IPSP_A$ recovery in CDC-ACSF 5 mM K^+, after reduction of $[K^+]_o$ to 2.5 mM (left columns), and during application of 2.5 mM K^+ plus 2.5 mM Cs^+ in CDC-ACSF (right columns).

values even more (97%). Correspondingly, neurones with a relatively high Cl^- extrusion rate exhibited slight rate changes on application of Cs^+, whereas Cs^+ had negligible effects in neurones with low rates (Fig. 15*B*). Segregating the effects of 9AC on τ in a similar fashion revealed that neurones with a small τ (<12 s, average 10.3 ± 0.9 s; $n = 3$) exhibited a 9AC-sensitive rate of 0.0105 s^{-1}, which is about one-third of rat values, while the neurones with large τ values (>12 s, average 17.5 ± 3.3 s, $n = 5$) exhibited a smaller ClC2 rate (0.0065 s^{-1}, i.e. about 20% of the rat 9AC-sensitive rate). In the series of bumetanide applications none of the neurones had τ values below 12 s, and we therefore arbitrarily used 15 s as a border. Three neurones exhibited τ values below 15 s (between 12.8 and 14.9 s, average 14.1 ± 1.1 s), and the recovery τ of the remaining neurones exceeded 20 s (range 21.6–24.5 s, average 22.5 ± 1.2 s, $n = 5$). The three neurones with intermediate τ values had a mean bumetanide-sensitive rate of 0.0287 ± 0.0011 s^{-1}, which is similar to that of rat neurones (0.0263 s^{-1}). The neurones with τ values exceeding 20 s had an average rate of 0.0049 ± 0.0050 s^{-1}, i.e. about 5-fold smaller than the group of neurones with intermediate τ values. From these data we envisage an initial decline in KCC2 (an 80% decrease in KCC2 alone would increase the τ to about 12 s) and subsequent or concomitant decline in ClC2 by 80% would increase the time constant to near 16 s. The reverse order of decline is unlikely since HENC neurones with τ values near 10 s have a slightly smaller (68%) reduction in their ClC2-mediated rate, compared to KCC2, which is decreased by 82%. NKCC1 decreases last in this putative sequence of events since neurones with intermediate τ values (below 15 s) had normal NKCC1-mediated rates. A decrease in NKCC1 may cause the τ values between 20 and 30 s (see Fig. 9*A*). In fact, segregating the bumetanide data into two groups reveals that the group with τ values >20 s exhibited no significant change in τ on application of bumetanide (control: 22.5 ± 1.2 s, bumetanide: 24.1 ± 4.6 s; $n = 5$ $P > 0.05$).

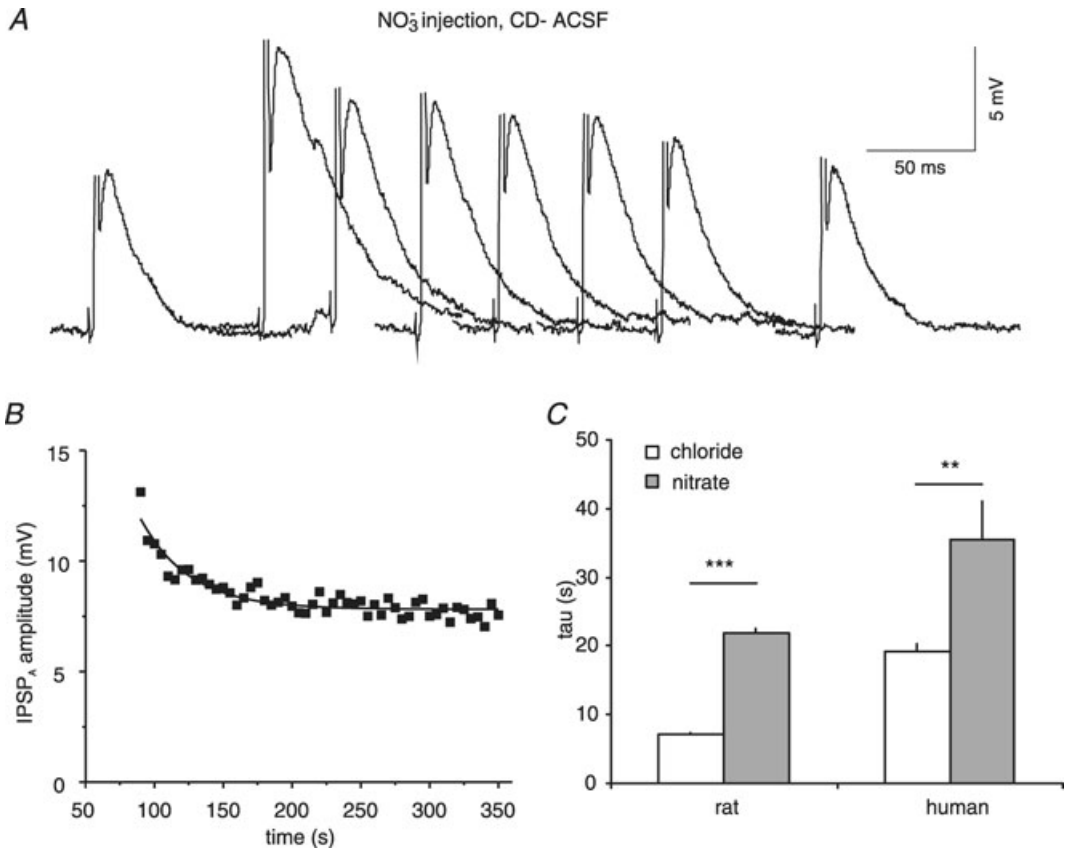

Figure 13. $IPSP_A$ recovery following NO_3^- injections in HENC neurones
A, traces of pharmacologically isolated $IPSP_A$ obtained before and at 0, 10, 20, 30, 40, 50 and 260 s after cessation of NO_3^- injection. The amplitude may have been slightly affected by the initial AP (truncated). The time scale refers to the individual traces. Traces have been partly superimposed. *B*, plot of the $IPSP_A$ amplitude mean values from 6 injections in the neurone shown in panel *A*. The curve represents an exponential fit to the data points indicating a τ of decay of 34.2 s. *C*, comparison of $IPSP_A$ recovery τ values from Cl^- or NO_3^- injections in rat and HENC neurones as indicated.

The group with intermediate τ values (14.1 ± 1.1 s) had a significantly smaller τ ($P < 0.001$) than the other group and exhibited a significant increase to 23.9 s ± 3.6 s ($n = 3$, $P < 0.05$). Interestingly, the values of these two groups in the presence of bumetanide were indistinguishable ($P > 0.05$). In this context it should be pointed out that only 16 neurones had τ values in the range of rat neurones (Fig. 9*A*), i.e. below 12 s, whereas 20 neurones exhibited τ values between 12 and 20 s, and in 24 neurones tau exceeded 20 s.

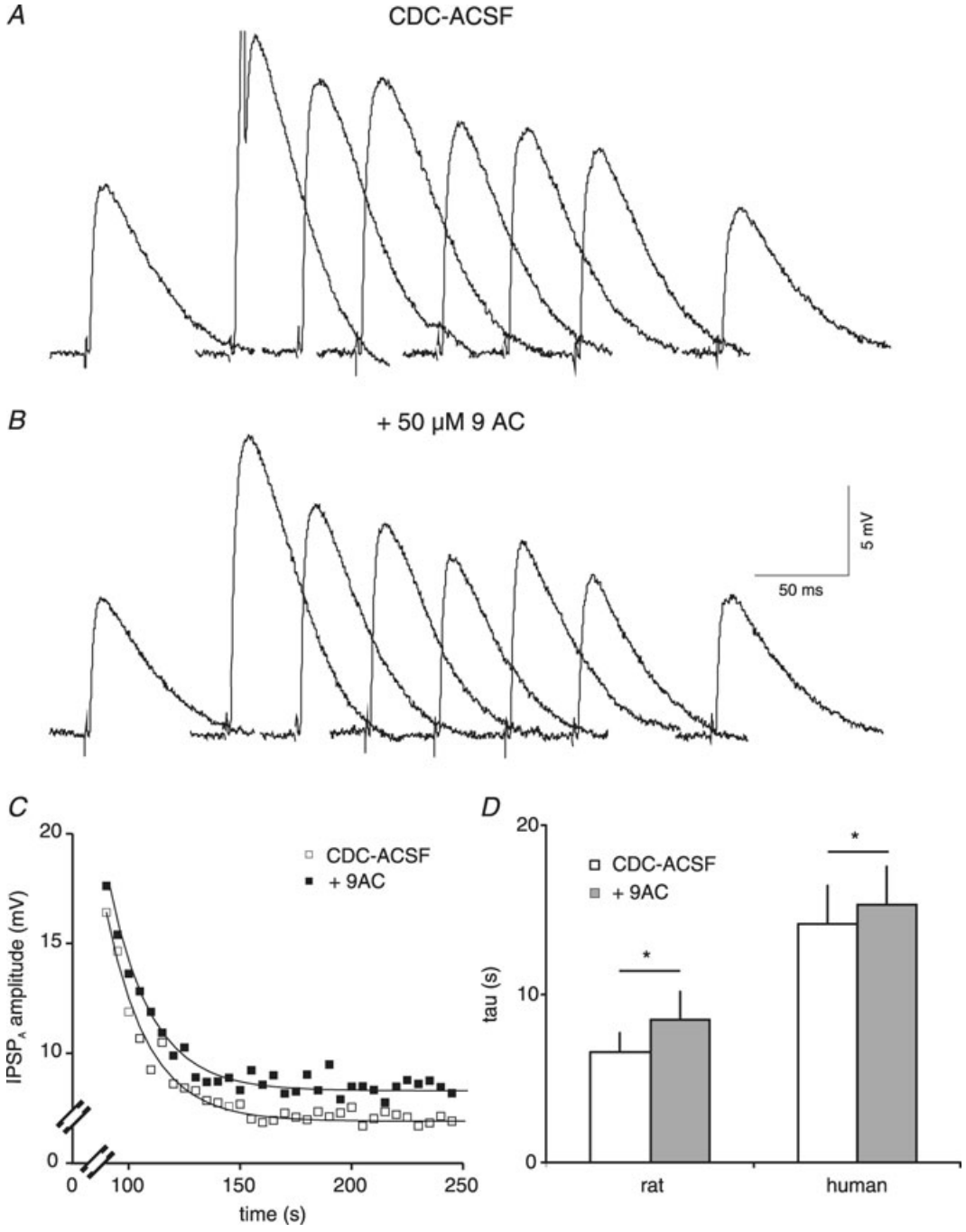

Figure 14. Effects of 9AC on HENC neurones
A and *B*, traces of $IPSP_A$ from a HENC neurone in CDC-ACSF (*A*) and in the presence of 50 μM 9AC (*B*). The time scale refers to the individual traces. The traces before and at 0, 5, 10, 15, 20, 25 and 260 s after end of Cl^- injection have been partly superimposed. *C*, plot of the average $IPSP_A$ amplitude from three consecutive Cl^- injections in CDC-ACSF (open squares) and CDC-ACSF plus 50 μM 9AC (filled squares). The curves represent the exponential fits to the data points with τ values of 17.6 s and 18.7 s, respectively. *D*, plot of the mean values of recovery time constant in CDC-ACSF and after addition of 9AC in rat and HENC neurones.

Table 2. Time constants of recovery of TLE neurones under the different experimental condition

Condition	τ (s)	Rate (s^{-1})	Isol. rates (s^{-1})	Calculation of rates for the different pathways			
ACSF	20.32 ± 11.38 (85)	0.0492					
CDC-ACSF	19.02 ± 9.63 (62)		0.0526				0.0526
CDC-ACSF	19.36 ± 4.48 (8)	0.0517					
With bumet.	24.05 ± 3.15 (8)	0.0416	0.0101	0.0101			−0.0101
CDC-ACSF	15.45 ± 6.02 (8)	0.0647					
With furos.	44.10 ± 11.43 (8)	0.0227	0.0420				
CDC-ACSF	14.80 ± 4.47 (8)	0.0676					
With 9AC	16.45 ± 4.95 (8)	0.0608	0.0068		0.0068	−0.0056*	−0.0068
CDC-ACSF-5 mM K^+	15.04 ± 4.69 (9)	0.0665					
CDC-ACSF-2.5 mM Cs^+	17.48 ± 5.97 (9)	0.0572	0.0093				
CDC/nitrate	35.48 ± 17.29 (7)	0.0282	0.0282			0.0282	−0.0226
			rate	0.0101	0.0068	0.0226	0.0132
			pathway	NKCC1	ClC2	AE	KCC2

The time constants in control CDC-ACSF differ for some of the subgroups from the ensemble average. The rates were therefore calculated for each experimental group as difference in rate with and without the drugs. On the right hand the calculations of the rates of individual pathways are presented. To obtain the estimate for the AE, the NO_3^- rate of ClC2 has to be subtracted (see Table 1). To compensate for the lack of NO_3^- transport rate via ClC2, a calculated NO_3^- extrusion rate (indicated by the asterisk) was used (ClC2 rate for Cl^- multiplied by 0.83, determined experimentally in rat neurones).

Discussion

Two main interrelated conclusions emerge from the data presented. Firstly, in about half of the HENC neurones, the $E_{IPSP\text{-}A}$ was much less negative (−55 mV) than in the other half (−69 mV). Secondly, Cl^- extrusion in HENC neurones was much slower (average τ: 19 s) compared to rat cortical neurones (τ: 7 s) and exhibited a much larger variability between neurones.

Before discussing the cellular mechanisms underlying these two phenomena, we should briefly reiterate inherent problems in studying human tissue. The patients suffered years of epilepsy before operation, on average for about 20 years in the cases we investigated. Moreover, the patients had various medications that did not adequately control seizure activity. Human control tissues from tumour resections without seizure history were not available for the experiments in this study. The validity of comparison of data from human neurones with that from the rat may be debatable, although rodent neurones have provided indispensable data concerning the properties of channels and receptors in the healthy cortex as a reference for human tissues (Na^+ currents: Cummins *et al.* 1994; H-currents: Wierschke *et al.* 2010; $GABA_A$ receptors: Gibbs *et al.* 1996; $GABA_B$ receptors: Teichgräber *et al.* 2009). As far as possible, human and rat tissue were treated in the same way in this study. Our data from rat neurones were by and large similar to those from various species (Connors *et al.* 1988; Thompson *et al.* 1988*a*; Deisz & Prince, 1989; Kaila *et al.* 1993; Luhmann & Prince, 1991). It could be argued that resected human tissue may suffer transient ischaemia and/or trauma during surgery, transport and slicing. Transient ischaemia may increase $[Cl^-]_i$ as inferred from fluorometric measurements (Pond *et al.* 2006). Neuronal trauma is also capable of inducing a depolarizing shift of $GABA_A$ responses (van den Pol *et al.* 1996). However, both normal and depolarized $E_{IPSP\text{-}A}$ were observed in slices of a given human tissue. In addition, the HENC neurones appear to be fairly tough since E_m and AP amplitudes were in the range typical of cortical neurones for astounding periods (often 24 h, Teichgräber *et al.* 2009). Therefore, we conclude that the depolarizing $GABA_A$ receptor-mediated responses represent a crucial phenomenon of the human epileptogenic tissue. This view is supported by a previous report of depolarizing $GABA_A$ responses in slices of resected human subiculum correlating with interictal activity *in vivo* (Cohen *et al.* 2002).

Depolarizing $GABA_A$ receptor-mediated responses in human epileptogenic cortex

Given the conclusion that the depolarizing $E_{IPSP\text{-}A}$ is related to the pathophysiology of epilepsy *in vivo*, a delineation of the underlying mechanisms may improve therapeutic strategies. The key question therefore concerns the mechanism governing an $E_{IPSP\text{-}A}$ near −55 mV, observed in about half of the HENC neurones. Two contending mechanisms, not mutually exclusive, have been proposed, namely, a decreased function (or number) of KCC2 transporters (Deisz *et al.* 1998) and an up-regulation of, presumed inwardly directed, NKCC1 transporters (Palma *et al.* 2006). The study by Palma *et al.* (2006) provided some mRNA data indicating a relative

dominance of NKCC1 *vs.* KCC2 expression in human epileptogenic subiculum (see below).

Our data suggest that in HENC neurones several Cl^- transport mechanisms are reduced. Such a change would be undetectable in patch-clamp recordings (Gibbs *et al.* 1996), since $[Cl^-]_i$ is governed by the filling solution of the patch electrode rather than by the physiological transport across the membrane. Before discussing the pharmacology of Cl^- homeostasis, we briefly consider the possible ionic mechanisms underlying the depolarizing $IPSP_A$. Given a relative Cl^-:HCO_3^- permeability of $GABA_A$ receptors of 1:0.2 (Kaila *et al.* 1993), the GHK equation allows calculation of $[Ci^-]_i$ and ECl. The mean $E_{IPSP\text{-}A}$ of the 'normal' group of HENC neurones (−68.8 mV) yields a $[Cl^-]_i$ of 6.9 mM corresponding to an E_{Cl} of −77.8 mV. Thus E_{Cl} is about 6 mV more negative than E_m (−71.5 mV) and $[Cl^-]_i$ about 2 mM lower than predicted by a passive distribution. The $E_{IPSP\text{-}A}$ of the second group (−55.2 mV), however, cannot be explained by a passive Cl^- distribution, assuming an unaltered permeability ratio and $E_{bicarbonate}$. The calculation yields an E_{Cl} of −59.7 mV (at constant intracellular HCO_3^-), about 10 mV less negative than E_m and a $[Cl^-]_i$ of 13.7 mM about 5 mM higher than predicted by a passive distribution. Hence, either inward Cl^- transport or an increased $[HCO_3^-]_i$ must underlie the more depolarizing $E_{IPSP\text{-}A}$. Considering that inward transport by NKCC1 is slow (Achilles *et al.* 2007) and NKCC1 is reduced in HENC tissues (on average by 62%), inward Cl^- transport via NKCC1 appears unlikely. To account for the $E_{IPSP\text{-}A}$ of −55 mV with passive Cl^- distribution, either a $[HCO_3^-]_i$ of near 40 mM or an altered relative permeability of Cl^-: HCO_3^- of 1:0.6 would be required, which is even less likely. Thus the presence of unaltered NKKC1-mediated rate in HENC neurones with intermediate τ values, when transport via KCC2 and ClC2 is greatly reduced (by 80%), may contribute to $E_{IPSP\text{-}A}$ values less negative than −64 mV. This value could be set by a passive Cl^- distribution (E_m of −71.5 mV) and the partial HCO_3^- permeability of $GABA_A$ receptors (Kaila *et al.* 1993).

The question then arises, which of the pathways can maintain E_{Cl} sufficiently negative to yield an $E_{IPSP\text{-}A}$ near E_m despite HCO_3^- permeability? From a thermodynamic viewpoint NKCC1 is not capable of maintaining low $[Cl^-]_i$ since the equilibrium of NKCC1-mediated transport is near −40 mV (Brumback & Staley, 2008). Regarding ClC2, the channels are activated by hyperpolarization (Clark *et al.* 1998), half-maximally at 15 mV more negative than E_{Cl} (Staley, 1994). However, this prerequisite for ClC2 contributing to a net Cl^- efflux (E_m much less negative than E_{Cl}) is hardly present in adult cortical neurones in steady state. Therefore, we favour KCC2 as the key pathway maintaining low $[Cl^-]_i$ since the coupling of Cl^- extrusion to the K^+ gradient could push E_{Cl} to near −90 mV (Alvarez-Leefmans, 1990).

Kinetics and pharmacology of anion transport in neocortical neurones

First, we will discuss the data obtained during parallel experiments on rat cortical neurones. In essence, we corroborated and extended previous data from guinea pig cortex (Thompson *et al.* 1988*a*,*b*). Despite different methods employed here (e.g. ether anaesthesia, submerged-type recording chamber, different cortex and cortical layers and 32°C) compared to the previous

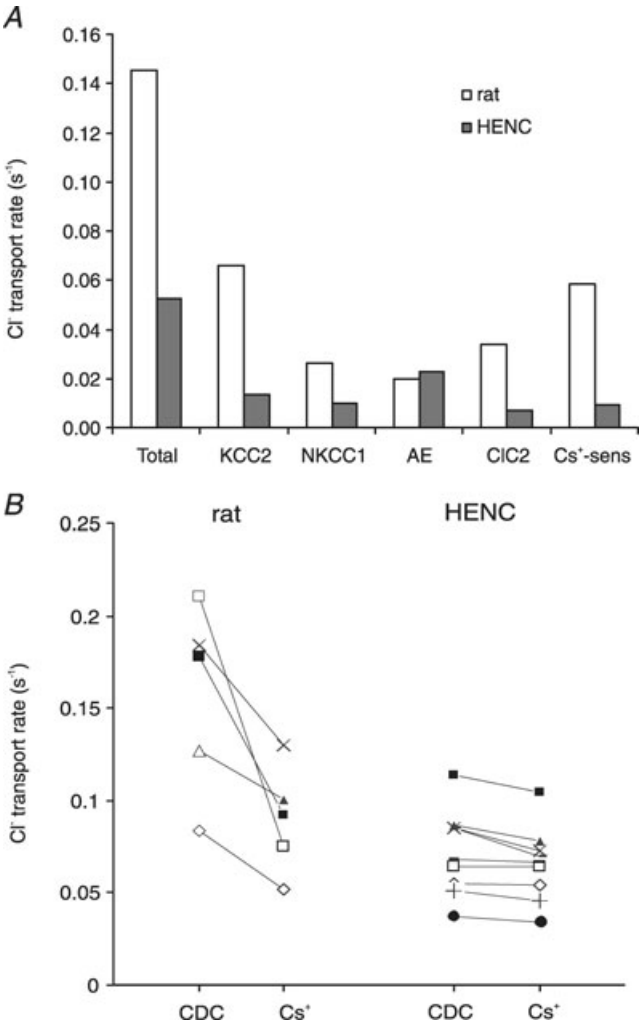

Figure 15. Average rates of chloride extrusion in rat and HENC neurones
A, plot of the rates of Cl^- extrusion obtained in rat and HENC neurones. The columns represent the rates of the total Cl^- extrusion and the rates via the various pathways calculated according to eqns (1)–(5). The open and filled columns represent data from rat and HENC neurones, respectively. A graphical representation of the S.E.M. is not given since some values (KCC2 and AE) can only be calculated from the mean τ values. *B*, plot of the change in Cl^- extrusion rate in individual rat and HENC neurones on application of 2.5 mM Cs^+. Four HENC neurones with relatively high extrusion rates exhibited slight effects of Cs^+ while five neurones with relatively lower rates in CDC-ACSF showed marginal effects.

experiments (pentobarbitone anaesthesia, interface-type recording chamber), the τ values (7.9 s in ACSF) obtained are similar to those in neocortical neurones from guinea pig (τ 6.9 s at 36.5°C and 11 s at 32°C, Thompson *et al.* 1988*a*) and rat (Sprague–Dawley: τ 6.8 s at 35°C; Luhmann & Prince, 1991). Application of furosemide caused a marked slowing of recovery from Cl^- loading, consistent with a large body of evidence indicating a reduced Cl^- outward transport in the presence of furosemide in various neurones (Deisz & Lux, 1982; Misgeld *et al.* 1986; Thompson *et al.* 1988*a*; Jarolimek *et al.* 1999; DeFazio *et al.* 2000). We also observed a marked shift of the $E_{IPSP\text{-}A}$ from −62 mV to −54 mV, providing direct evidence that some furosemide-sensitive pathways maintain low $[Cl^-]_i$ despite a constant load from the KCl in the recording electrode.

The significant slowing of recovery by bumetanide, similar to previous data (Thompson *et al.* 1988*b*), implies that a bumetanide-sensitive transporter, i.e. NKCC1, participates in Cl^- extrusion. However, determination of the $E_{IPSP\text{-}A}$ with KCl-filled electrodes revealed no significant change by bumetanide. These two findings together suggest that bumetanide only affects the kinetics of Cl^- extrusion at high levels of $[Cl^-]_i$ such as those reached during iontophoresis, but not the net outward transport of Cl^- at more moderate levels. In contrast to the view that bumetanide-sensitive transporters exclusively mediate inward transport of Cl^-, we propose that NKCC1 contributes to outward Cl^- transport.

K^+ dependence of Cl^- outward transport

Direct evidence for the presence of a K^+-coupled transporter was obtained from the decreased recovery τ of the isolated $IPSP_A$ caused by reducing $[K^+]_o$ (from 5 mM to 2.5 mM; see also Thompson *et al.* 1988*a*). Further evidence for a K^+-sensitive outward transport was provided by the Cs^+ experiments. Cs^+, like NH_4^+, causes a reversible shift of the E_{IPSP} towards resting E_m (Aickin *et al.* 1982). Unlike NH_4^+, which is carried by KCC2 (Liu *et al.* 2003; Williams & Payne, 2004) thereby causing complicating intracellular pH changes (Williams & Payne, 2004; Titz *et al.* 2006), Cs^+ decreases net outward transport by reducing the maximal velocity of KCC2-mediated transport (Williams & Payne, 2004). Our data demonstrating that 2.5 mM Cs^+ (equimolar replacement of K^+) increased the τ of recovery from 7.1 s to 12.2 s is in line with this notion and in turn indicates the presence of KCC2 in rat cortical neurones.

Contribution of AE and ClC2 to Cl^- extrusion

In addition to KCC2 and NKCC1, we also evaluated the contribution of less selective routes of anion movement by injecting NO_3^-. Two likely unselective pathways (AE and ClC2) have been established in the CNS by immunohistochemical methods (Havenga *et al.* 1994; Sik *et al.* 2000). Some evidence for the participation of AE in the unselective clearance of anion loads is provided by the increased time constant of recovery following NO_3^- injection in the presence of furosemide (see Brazy & Gunn, 1976).

However, NO_3^- clearance may not be confined to AE. Some members of the ClC family also allow permeation of NO_3^- (Fahlke, 2001) and isoforms expressed in retinal cones have even better permeability for NO_3^- than for Cl^- (Wilson & Gleason, 1991). The slowing of NO_3^- clearance by the established ClC blocker 9AC (Clark *et al.* 1998) indicates that ClC2 also participates in NO_3^- clearance from rat neurones. However, application of 9AC had no effect on the steady state of $E_{IPSP\text{-}A}$ (see Fig. 4) despite continuous Cl^- leakage from the electrode. This renders it unlikely that a decrease in ClC2 *per se* is the crucial mechanism for generation of the depolarizing $E_{IPSP\text{-}A}$ (cf. Mladinic *et al.* 1999). A decrease in ClC2 will only have profound effects in the presence of inward Cl^- transport. This is best illustrated by the massive increase in $[Cl^-]_i$ in rat lumbrical muscle cells on application of 9AC (Aickin *et al.* 1989). Our view that a decrease in ClC2 does not cause the depolarizing $E_{IPSP\text{-}A}$ *per se* and hence does not constitute a crucial mechanism of epilepsy is in line with previous observations demonstrating that ClC2 knockout animals do not present with seizures (for review see Jentsch *et al.* 2005). However, despite the unaltered $E_{IPSP\text{-}A}$ in the presence of 9AC, the same amount of Cl^- injection caused a roughly twofold larger increase in $[Cl^-]_i$, indicating that 9AC-sensitive components limit the efficacy of Cl^- loading. Presumably, the hyperpolarization caused by current injection together with a depolarizing shift of E_{Cl} provides a sufficient driving force for loss of Cl^- via ClC2. Finally, ClC2-mediated currents in rat sympathetic neurones are about 300 pA (at −100 mV; Clark et al, 1998). Since the cortical neurones are hyperpolarized into this range by injection of 1 nA, about half of the injected Cl^- might immediately escape via ClC2 (half of the current is carried by K^+).

Relative rates of chloride extrusion in rat cortical neurones

Various pharmacological conditions were used to estimate the rates of Cl^- efflux mediated by the pathways KCC2, NKCC1, AE and ClC2. The simplifying assumptions underlying the estimates are: (1) the changes in $IPSP_A$ amplitude reflect changes in the concentration of intracellular anions; (2) both AE and ClC2 carry Cl^- and NO_3^-; (3) bumetanide selectively antagonizes NKCC1 (e.g. Titz *et al.* 2006); (4) furosemide reduces AE, KCC2 and NKCC1; and (5) the effectiveness of the drugs is comparable in rat and HENC neurones. The calculations yield relative rates

in rat neurones (see Table 1) indicating a dominance of KCC2-mediated fluxes (45.3% of the total rate) compared to NKCC1 (18.1%), AE (13.6%) and ClC2 (23.1%).

We tested the validity of our estimates by comparing data obtained with different approaches. For instance, the results of the Cs^+ experiments support our estimates. The Cs^+-sensitive flux rate of 0.0584 s^{-1} was close to the estimate for KCC2 (0.0659 s^{-1}) obtained using eqn (5). In addition, the total rate obtained from Cl^- injections minus the 'unselective rate' obtained from NO_3^- injections yielded the 'selective' flux, presumably mediated by NKCC1 and KCC2. The rate obtained for the selective routes (0.0981 s^{-1}) is similar to the rate estimated from two other independently obtained rates, namely the sum of bumetanide-sensitive and Cs^+-sensitive rates (0.0847 s^{-1}). These simplified estimates may underestimate some of the transport rates due to incomplete blockade by the drug applications. Some clues concerning the magnitude of blockade can be obtained from the furosemide effects on the AE. The rate of the AE (see Table 1) amounted to 0.0197 s^{-1} in CDC-ACSF and 0.0125 s^{-1} in the presence of furosemide; thus furosemide reduced the flux rate to 63%. Whether the other targets of furosemide (KCC2 and NKCC1) are reduced to a similar extent would require further experiments. Overall, the agreement of six independent experimental conditions (Cl^- injections, NO_3^- injections, bumetanide, furosemide, 9AC and Cs^+ applications) indicates that the estimates are reliable.

Properties of Cl^- extrusion in HENC neurones

Injection of Cl^- into HENC neurones caused a marked increase in the amplitude of the isolated $IPSP_A$. The estimated $E_{IPSP\text{-}A}$ decreased from −59.5 mV to −48.0 mV on injection of 1 nA for 1 min, corresponding to an increase in $[Cl^-]_i$ from 11.8 mM to 19.8 mM. Steady state E_m and $E_{IPSP\text{-}A}$ values were indistinguishable from those in rat neurones ($P > 0.05$). However, the effects of iontophoresis differed markedly. The maximal $[Cl^-]_i$ was much higher (19 mM) in HENC neurones (compared with 14 mM in rat) and increases over the preceding control were almost twice as large in HENC neurones (by 7.9 mM; rat: by 4.5 mM). The amplitude of the $IPSP_A$ gradually recovered, but the τ (19 s) was almost 3-fold larger than in rat neurones (7 s). Moreover, the τ values varied considerably between HENC neurones (range 8.0–48.0 s in CDC-ACSF, see Fig. 9*A*), compatible with a variable impairment of Cl^- transport (see below). This variability is not only due to differences between resections, but rather represents an intra-individual variability of Cl^- regulation. In fact, neurones with τ values below or above 11.5 s were obtained in 14 of 29 resections, similar to the variability of $E_{IPSP\text{-}A}$. Interestingly, an impaired Cl^- regulation was reported in a cortical lesion model associated with hyperexcitability (Jin *et al.* 2005).

Pharmacology of Cl^- transport in HENC neurones

Of particular interest were the effects of the selective NKCC1 blocker bumetanide on $E_{IPSP\text{-}A}$ and on the kinetics of Cl^- extrusion. Considering the proposed upregulation of NKCC1 in human epileptogenic subiculum (Palma *et al.* 2006), a marked effect of bumetanide might be anticipated, if only bumetanide-sensitive transporters, i.e. NKCC1, are upregulated. An accelerated recovery by bumetanide might even be expected in HENC neurones if an inward Cl^- transport via NKCC1 exceeds Cl^- extrusion. Instead, bumetanide caused a further slowing of the recovery in HENC neurones, with τ increasing on average from 19.4 s to 24.0 s. This suggests that a bumetanide-sensitive process, i.e. involving NKCC1, participates in Cl^- outward transport, at least at the high $[Cl^-]_i$ attained during injections. Yet $E_{IPSP\text{-}A}$ and $[Cl^-]_i$ were unaltered (CDC-ACSF: −57.2 mV, bumetanide: −57.6 mV, corresponding to $[Cl^-]_i$ of 12.5 mM and 12.2 mM, respectively). The average values of τ are misleading, though, because two subgroups could be distinguished. Neurones with τ values below 15 s exhibited a marked increase, whereas neurones with τ values above 20 s exhibited on average no significant effect of bumetanide. Calculating the rates revealed that neurones with average τ values below 15 s had a bumetanide-sensitive rate similar to rat neurones, and the neurones with large τ values had a greatly reduced bumetanide-sensitive rate (by 82%), i.e. a much smaller NKCC1 component.

The effects of furosemide on the τ of recovery from Cl^- injections in HENC neurones (Fig. 11*D*) at first sight appear in line with a wealth of evidence indicating a reduced Cl^- extrusion by furosemide (Deisz & Lux, 1982; Misgeld *et al.* 1986; Thompson *et al.* 1988*a*; Jarolimek *et al.* 1999). This view would be in line with the shift in $E_{IPSP\text{-}A}$ (from −61.1 mV to −49.4 mV). Yet the magnitude of the furosemide effect (increase of τ from 15.5 s to 44.1 s, rat from 7.1 s to 16.6 s) was puzzling, since a complete block of KCC2, NKCC1 and AE would increase the recovery τ to maximally 30 s, rather than 44 s. However, in HENC neurones ClC2 is also reduced and the relative rates of Cl^- efflux are shifted towards a dominance of AE (from 13.6% to 43%). This shift in the relative contribution, in fact, accounts for the marked effect of furosemide on the recovery τ of HENC neurones (see below).

Effects of altered $[K^+]_o$ and of Cs^+ application

Changes in $[K^+]_o$ are widely used to test the involvement of K^+-dependent Cl^- transport (Aickin *et al.* 1982; Deisz

& Lux, 1982; Thompson *et al.* 1988*a*; Jarolimek *et al.* 1999). The unaltered Cl^- extrusion in HENC neurones upon reduction of $[K^+]_o$ suggests that a deficit of K^+-dependent transporters contributes to the slow time course of Cl^- extrusion. Further evidence was provided by Cs^+ application which is known to reduce the maximal velocity of KCC2-mediated transport (Williams & Payne, 2004). The small but significant increase in τ therefore indicated, firstly, the presence of a Cs^+-sensitive KCC2, and, secondly, that KCC2 is relatively small in HENC neurones. Interestingly, in cultured rat midbrain neurones, Cs^+ has no effect on dendritic Cl^- homeostasis (Jarolimek *et al.* 1999), perhaps due to a paucity of KCC2, as in dendrites of hippocampal CA1 neurones (Misgeld *et al.* 1986).

Contribution of AE and ClC2 to anion extrusion in HENC neurones

Given our assumption that NO_3^- clearance is mediated mainly by 'unselective' pathways, the observed slow recovery from NO_3^- loading in HENC neurones (τ: 35.5 s *vs.* 21.1 s in rat neurones) indicates that these pathways are less effective in HENC neurones. Since the τ of Cl^- recovery was only slightly increased by 9AC in HENC neurones, it seems most likely that NO_3^- efflux via CIC2 had been reduced. Together, these data indicate that (i) a crucial deficit of Cl^- extrusion in HENC neurones relates to the reduced 9AC-sensitive component and (ii) 9AC-sensitive transport, i.e. ClC2, does not likely alter the steady state, and hence cannot account for the depolarizing $E_{IPSP\text{-}A}$ observed in HENC neurones.

The relative contribution of pathways to Cl^- extrusion in HENC neurones

The rates of individual Cl^- pathways in HENC neurones were calculated analogous to those in rat cortical neurones. First of all, the total rate of Cl^- extrusion was 63.8% smaller than in rat neurones (see Table 2). However, the difference in rate between rat and HENC neurones ($0.0930\ s^{-1}$) is larger than the estimated rate provided by KCC2 in rat neurones ($0.0659\ s^{-1}$), indicating that other transporters must be reduced as well. We verified that a decrease in KCC2 alone cannot account for the observed slow recovery in HENC neurones as follows: using the transport rates of AE, ClC2 and NKCC1 estimated in rat neurones, an 80% decrease in the KCC2-mediated rate alone yields a time constant of 10.8 s, considerably smaller than the 19.0 s actually observed in HENC neurones.

Comparison of the data presented in Tables 1 and 2 reveals that the NKCC1- and ClC2-mediated rates were also smaller than in rat neurones (by 61.7% and 79.9%, respectively). These marked decreases also change the relative contribution of transporters to Cl^- homeostasis in HENC neurones; KCC2, NKCC1, AE and ClC2 comprise on average 25.0%, 19.2%, 43.0.0% and 12.9% of the total flux, respectively. This change in the relative rates of the different pathways, in particular the dominance of the AE flux, which increased from 13.6% to 43.0%, probably accounts for the peculiar pharmacology, i.e. the marked effect of furosemide on HENC neurones. This view is supported by calculating a theoretical furosemide effect. Assuming furosemide causes a 65% reduction in the rates of KCC2, NKCC1 and AE in both species, the calculated τ increases to 13.7 s in rat neurones and to 46.2 s in HENC neurones. These calculated τ changes are remarkably similar to experimental data in the presence of furosemide (rat neurones: τ increased to 16.6 s; HENC neurones: increased to 44.1 s).

The change in rate on application of bumetanide indicates that NKCC1-mediated transport of HENC neurones was on average 62% smaller than in rat neurones (see Tables), which is at variance with the proposed up-regulation of NKCC1 (Palma *et al.* 2006). These authors provided mRNA data indicating a relative dominance of NKCC1 *vs.* KCC2 expression in human epileptogenic tissue. However, the functional evidence obtained by determining the GABA reversal potentials is debatable, since *Xenopus* oocytes injected with membrane fragments of human tissue were used. The stability, transport to and emplacement of human proteins into the oocyte membrane may differ from the physiological situation in native neurones. In particular, the probability of NKCC1 and KCC2 emplacement into the heterologous membrane may cause a different ratio of the two transporters compared to membranes of intact neurones. Hence, the proposed functional dominance of NKCC1-mediated inward transport in oocytes may not necessarily reflect the physiological ratio of transporters, but rather the likelihood of protein insertion into the membrane.

In any case, our evidence indicating a 62% smaller NKCC1 rate in HENC *vs.* rat neurones compared to the 80% decrease of flux rate mediated by KCC2 would tend to change the ratio of KCC2- *vs.* NKCC1-mediated fluxes from approximately 2.5:1 to 1.3:1 (see Tables). This altered ratio appears to be in line with the proposed altered balance between KCC2 and NKCC1 in human subiculum (Palma *et al.* 2006) by up-regulation of NKCC1. However, our data indicate that NKCC1 is considerably reduced rather than up-regulated, but by a smaller degree than KCC2.

Implications for drug therapy of epilepsy

This conclusion has important implications for a therapeutic use of bumetanide. Dzhala *et al.* (2005)

and Huberfeld *et al.* (2007) inferred that bumetanide may be a useful anticonvulsant due to its blocking of NKCC1-mediated inward transport (cf Kilb et al. 2007). At least in the adult neocortex, this approach might be of little benefit or even increase the probability of seizures. Unlike early postnatal stages with high NKCC1 and low KCC2 expression (Dzhala *et al.* 2005), in adult HENC neurones, NKCC1 is reduced below the adult level required for normal function. In fact, bumetanide further slows recovery from Cl^- loading in HENC neurones (mean 30% increase of τ). This slowed recovery of the $IPSP_A$ in the presence of bumetanide implies that after a pathophysiological Cl^- load, the gradient of $GABA_A$ receptor-mediated inhibition is less effective much longer, which, in turn, would facilitate excess activity during subsequent synaptic activation.

These considerations are of particular relevance with regard to the proposed temporal sequence of changes in Cl^- pathways. From the different magnitudes of Cs^+, 9AC and bumetanide effects on HENC neurones with different τ values, we propose an initial decline of KCC2 accompanied or followed by a decrease of ClC2, and, finally, of NKCC1 as well. The average reduction of NKCC1 by 62% in HENC neurones, when KCC2 and ClC2 are reduced by 80%, strongly argues against a clinical use of bumetanide in adult epilepsy patients. This view is substantiated by bumetanide effects on individual neurones. Neurones with a large τ (average 22 s) have no significant effect of bumetanide, yet neurones with intermediate τ values (14.1 s) have a large increase of τ (to 23.9 s). Thus bumetanide would have severe effects, further reducing the Cl^- transport capacity of neurones with intermediate τ values.

Our view of a more pronounced decrease of KCC2 *vs.* NKCC1 may relate to immunohistochemical data from human epileptogenic hippocampus (Munoz *et al.* 2007). In all hippocampal subfields (CA1–CA3) the NKCC1 immunosignal (IS) was similar to autopsy tissue, indicating unaltered rather than up-regulated NKCC1. However, in the subiculum and area CA1 a considerable fraction of neurones (20%) exhibited NKCC1-IS but no KCC2-IS, yet 93% of neurones exhibiting KCC2-IS also exhibited NKCC1-IS. We take this to indicate that NKCC1-IS is more robust than KCC2-IS, compatible with the above hypothesis.

Finally, impaired Cl^- outward transport must also be discussed with regard to the temporal properties of inhibition. Firstly, the $IPSP_A$ of HENC neurones exhibits little frequency-dependent depression due to a low density of $GABA_B$ receptors (Teichgräber *et al.* 2009), which would facilitate repetitive activity via depolarizing $GABA_A$ receptor-mediated responses in focal areas. A frequency-dependent depression of inhibition by presynaptic $GABA_B$ receptors (Deisz & Prince, 1989) in perifocal human neurones with properties similar to rodent cortex would facilitate recruitment of both adjacent perifocal and distant connected neurones. Secondly, the large recovery τ in HENC neurones would further alter temporal properties of inhibition: recovery from a given Cl^- load would be slowed, and thus inhibition would be less effective for prolonged periods of time.

In conclusion, our data provide evidence for a depolarizing $GABA_A$ receptor-mediated response in about half of the HENC neurones due to reduced Cl^- fluxes mediated by KCC2, NKCC1 and ClC2. The approximately 50:50 ratio of normal and depolarized $GABA_A$ reversal potentials may contribute to pharmacoresistance, since drugs augmenting $GABA_A$ receptors would exert little net effect.

References

Achilles K, Okabe A, Ikeda M, Shimizu-Okabe C, Yamada J, Fukuda A, Luhmann HJ & Kilb W (2007). Kinetic properties of Cl^- uptake mediated by Na^+-dependent K^+-$2Cl^-$ cotransport in immature rat neocortical neurons. *J Neurosci* **27**, 8616–8627.

Aickin CC, Betz WJ & Harris GL (1989). Intracellular chloride and the mechanism for its accumulation in rat lumbrical muscle. *J Physiol* **411**, 437–455.

Aickin CC, Deisz RA & Lux HD (1981). On the action of the anticonvulsant 5,5-diphenylhydantoin and the convulsant picrotoxin in crayfish stretch receptor. *J Physiol* **315**, 157–173.

Aickin CC, Deisz RA & Lux HD (1982). Ammonium action on post-synaptic inhibition in crayfish neurones: implications for the mechanism of chloride extrusion. *J Physiol* **329**, 319–339.

Alvarez-Leefmans FJ (1990). Intracellular Cl^- regulation and synaptic inhibition in vertebrate and invertebrate neurons. In *Chloride Channels and Carriers in Nerve, Muscle, and Glial Cells*, ed. Alvarez-Leefmans FJ & Russell JM, pp. 109–158. Plenum Publishing Corp., New York.

Ben-Ari Y (2002). Excitatory actions of GABA during development: the nature of the nurture. *Nat Rev Neurosci* **3**, 728–739.

Bormann J, Hamill OP & Sakmann B (1987). Mechanism of anion permeation through channels gated by glycine and gamma-aminobutyric acid in mouse cultured spinal neurones. *J Physiol* **385**, 243–286.

Brazy PC & Gunn RB (1976). Furosemide inhibition of chloride transport in human red blood cells. *J Gen Physiol* **68**, 583–599.

Brumback AC & Staley KJ (2008). Thermodynamic regulation of NKCC1-mediated Cl^- cotransport underlies plasticity of $GABA_A$ signaling in neonatal neurons. *J Neurosci* **28**, 1301–1312.

Clark S, Jordt S-E, Jentsch TJ & Mathie A (1998). Characterization of the hyperpolarization-activated chloride current in dissociated rat sympathetic neurons. *J Physiol* **506**, 665–678.

Cohen I, Navarro V, Clemenceau S, Baulac M & Miles R (2002). On the origin of interictal activity in human temporal lobe epilepsy in vitro. *Science* **298**, 1418–1421.

Connors BW, Malenka RC & Silva LR (1988). Two inhibitory postsynaptic potentials and $GABA_A$ and $GABA_B$ receptor-mediated responses in neocortex of rat and cat. *J Physiol* **406**, 443–468.

Cummins TR, Xia Y & Haddad GG (1994). Functional properties of rat and human neocortical voltage-sensitive sodium currents. *J Neurophysiol* **71**, 1052–1064.

DeFazio RA, Keros S, Quick MW & Hablitz JJ (2000). Potassium-coupled chloride cotransport controls intracellular chloride in rat neocortical pyramidal neurons. *J Neurosci* **20**, 8069–8076.

Deisz RA (1996). A tetrodotoxin-insensitive sodium current initiates burst firing of neocortical neurons. *Neuroscience* **70**, 341–351.

Deisz RA (1999*a*). The $GABA_B$ receptor antagonist CGP 55845A reduces presynaptic $GABA_B$ actions in neocortical neurons of the rat *in vitro*. *Neuroscience* **93**, 1241–1249.

Deisz RA (1999*b*). $GABA_B$ receptor-mediated effects in human and rat neocortical neurons in vitro. *Neuropharmacol* **38**, 1755–1766.

Deisz RA, Fortin G & Zieglgänsberger W (1991). Voltage dependence of excitatory postsynaptic potentials of rat neocortical neurones. *J Neurophysiol* **65**, 371–382.

Deisz RA, Lehmann T-N, Lanksch WR, Meencke HJ & Nitsch R (1998). Receptor mechanisms involved in hyperexcitability of cortical tissue from epilepsy surgery. *J Physiol* **513.P**, 35–36*P*.

Deisz RA, Lehmann T-N, Dehnicke C, Nitsch R (2008). Human cortical neurones in tissues from epilepsy surgery have a reduced chloride extrusion. *Proc Physiol Soc* **11**, C4.

Deisz RA & Lux HD (1977). Diphenylhydantoin prolongs post-synaptic inhibition and iontophoretic GABA action in the crayfish stretch receptor. *Neurosci Lett* **5**, 199–203.

Deisz RA & Lux HD (1982). The role of intracellular chloride in post-synaptic inhibition of crayfish stretch receptor neurones. *J Physiol* **326**, 123–128.

Deisz RA & Prince DA (1989). Frequency-dependent depression of inhibition in guinea-pig neocortex *in vitro* by $GABA_B$ receptor feedback on GABA release. *J Physiol* **412**, 513–541.

Delpire E (2000). Cation-chloride cotransporters in neuronal communication. *News Physiol Sci* **15**, 309–312.

Dzhala VI, Talos DM, Sdrulla DA, Brumback AC, Mathews GC, Benke TA, Delpire E, Jensen FE & Staley KJ (2005). NKCC1 transporter facilitates seizures in the developing brain. *Nature Med* **11**, 1205–1213.

Fahlke C (2001). Ion permeation and selectivity in ClC-type channels. *Am J Physiol Renal Physiol* **280**, F748–F757.

Gamba G (2005). Molecular physiology and pathophysiology of electroneutral cation-chloride cotransporters. *Physiol Rev* **85**, 423–493.

Gibbs JW 3rd, Zhang YF, Kao CQ, Holloway KL, Oh KS & Coulter DA (1996). Characterization of $GABA_A$ receptor function in human temporal cortical neurons. *J Neurophysiol* **75**, 1458–1471.

Granger P, Biton B, Faure C, Vige X, Depoortere H, Graham D, Langer SZ, Scatton B & Avenet P (1995). Modulation of the γ-aminobutyric acid type A receptor by the antiepileptic drugs carbamazepine and phenytoin. *Mol Pharmacol* **47**, 1189–1196.

Gutnick MJ, Connors BW & Prince DA (1982). Mechanisms of neocortical epileptogenesis in vitro. *J Neurophysiol* **48**, 1321–1335.

Havenga MJ, Bosman GJ, Appelhans H & De Grip WJ (1994). Expression of the anion exchanger (AE) gene family in human brain. Identification of a new AE protein: AE0. *Brain Res Mol Brain Res* **25**, 97–104.

Huberfeld G, Wittner L, Clemenceau S, Baulac M, Kaila K, Miles R & Rivera C (2007). Perturbed chloride homeostasis and GABAergic signaling in human temporal lobe epilepsy. *J Neurosci* **12**, 9866–9873.

Jentsch TJ, Steinmeyer K & Schwarz G (1990). Primary structure of *Torpedo marmorata* chloride channel isolated by expression cloning in *Xenopus* oocytes. *Nature* **348**, 510–514.

Jentsch TJ, Poet M, Fuhrmann JC & Zdebik AA (2005). Physiological functions of CLC Cl^- channels gleaned from human genetic disease and mouse models. *Annu Rev Physiol* **67**, 779–807.

Jin X, Huguenard JA & Prince DA (2005). Impaired Cl^- extrusion in layer V pyramidal neurons of chronically injured epileptogenic neocortex. *J Neurophysiol* **93**, 2117–2126.

Jarolimek W, Lewen A & Misgeld U (1999). A furosemide-sensitive K^+–Cl^- cotransporter counteracts intracellular Cl^- accumulation and depletion in cultured rat midbrain neurons. *J Neurosci* **19**, 4695–4704.

Kaila K, Voipio J, Paalasmaa P, Pasternack M & Deisz RA (1993). The role of bicarbonate in $GABA_A$ receptor-mediated IPSPs of rat neocortical neurones. *J Physiol* **464**, 273–289.

Kakazu Y, Akaike N, Komiyama S & Nabekura J (1999). Regulation of intracellular chloride by cotransporters in developing lateral superior olive neurons. *J Neurosci* **19**, 2843–2851.

Kilb W, Sinning A & Luhmann HJ (2007). Model-specific effects of bumetanide on epileptiform activity in the in-vitro intact hippocampus of the newborn mouse. *Neuropharmacol* **53**, 524–533.

Liu X, Titz S, Lewen A & Misgeld U (2003). KCC2 mediates NH_4^+ uptake in cultured rat brain neurons. *J Neurophysiol* **90**, 2785–2790.

Llinás R, Baker R & Precht W (1974). Blockage of inhibition by ammonium acetate action on chloride pump in cat trochlearis motoneurons. *J Neurophysiol* **37**, 522–532.

Luhmann HJ & Prince DA (1991). Postnatal maturation of the GABAergic system in rat neocortex. *J Neurophysiol* **65**, 247–263.

Lux HD (1971). Ammonium and chloride extrusion: hyperpolarizing synaptic inhibition in spinal motoneurons. *Science* **173**, 555–557.

Misgeld U, Deisz RA, Dodt HU & Lux HD (1986). The role of chloride transport in postsynaptic inhibition of hippocampal neurons. *Science* **232**, 1413–1415.

Mladinic M, Becchetti A, Didelon F, Bradbury A & Cherubini E (1999). Low expression of ClC-2 chloride channel during postnatal development: a mechanism for the paradoxical depolarizing action of GABA and glycine in the hippocampus. *Proc Biol Sci* **266**, 1207–1213.

Munoz, A, Méndez P, DeFelipe J & Alvarez-Leefmans FJ (2007). Cation-chloride cotransporters and GABA-ergic innervation in the human epileptic hippocampus. *Epilepsia* **48**, 663–673.

Palma E, Amici M, Sobrero F, Spinelli G, Di Angelantonio S, Ragozzino D, Mascia A, Scoppetta C, Esposito V, Miledi R & Eusebi F (2006). Anomalous levels of Cl^- transporters in the hippocampal subiculum from temporal lobe epilepsy patients make GABA excitatory. *Proc Natl Acad Sci U S A* **103**, 8465–8468.

Payne JA, Stevenson TJ & Donaldson LF (1996). Molecular characterization of a putative K-Cl cotransporter in rat brain. *J Biol Chem* **271**, 16245–16252.

Polc P & Haefely W (1976). Effects of two benzodiazepines, phenobarbitone, and baclofen on synaptic transmission in the cat cuneate nucleus. *Naunyn Schmiedebergs Arch Pharmacol* **294**, 121–131.

Pond BP, Berglund K, Kuner T, Feng G, Augustine GJ & Schwartz-Bloom RD (2006). The chloride transporter N^+-K^+-Cl^- cotransporter isoform-1 contributes to intracellular chloride increases after *in vitro* ischemia. *J Neurosci* **26**, 1396–1406.

Raabe W & Gumnit RJ (1975). Disinhibition in cat motor cortex by ammonia. *J Neurophysiol* **38**, 347–355.

Rice A, Rafiq A, Shapiro SM, Jakoi ER, Coulter D & DeLorenzo RJ (1996). Long-lasting reduction of inhibitory function and gamma-aminobutyric acid type A receptor subunit mRNA expression in a model of temporal lobe epilepsy. *Proc Natl Acad Sci U S A* **93**, 9665–9669.

Rivera C, Voipio J, Payne JA, Ruusuvuori E, Lahtinen H, Lamsa K, Pirvola U, Saarma M & Kaila K (1999). The K^+/Cl^- co-transporter KCC2 renders GABA hyperpolarizing during neuronal maturation. *Nature* **397**, 251–255.

Russell JM (2000). Sodium-potassium-chloride cotransport. *Physiol Rev* **80**, 211–276.

Sik A, Smith RA & Freund, TF (2000). Distribution of chloride channel-2-immunoreactive neuronal and astrocytic processes in the hippocampus. *Neuroscience* **101**, 51–65.

Staley K (1994). The role of an inwardly rectifying conductance in postsynaptic inhibition. *J Neurophysiol* **72**, 273–284.

Teichgräber LA, Lehmann T-N, Meencke H-J, Weiss T, Nitsch R & Deisz RA (2009). Impaired function of $GABA_B$ receptors in tissues from pharmacoresistant epilepsy patients. *Epilepsia* **50**, 1697–1716.

Thiemann A, Gründer S, Pusch M & Jentsch TJ (1992). A chloride channel widely expressed in epithelial and non-epithelial cells. *Nature* **356**, 57–60.

Thompson SM, Deisz RA & Prince DA (1988*a*). Relative contributions of passive equilibrium and active transport to the distribution of chloride in mammalian cortical neurons. *J Neurophysiol* **60**, 105–124.

Thompson SM, Deisz RA & Prince DA (1988*b*). Outward chloride/cation cotransport in mammalian cortical neurons. *Neurosci Lett* **89**, 49–54.

Titz S, Hormuzdi SM, Lewen A, Monyer H & Misgeld U (2006). Intracellular acidification in neurons induced by ammonium depends on KCC2 function. *Eur J Neurosci* **23**, 454–456.

van den Pol AN, Obrietan K & Chen G (1996). Excitatory actions of GABA after neuronal trauma. *J Neurosci* **16**, 4283–4292.

Wake H, Watanabe M, Moorhouse AJ, Kanematsu T, Horibe S, Matsukawa N, Asai K, Ojika K, Hirata M & Nabekura J (2007). Early changes in KCC2 phosphorylation in response to neuronal stress result in functional downregulation. *J Neurosci* **27**, 1642–1650.

Wierschke S, Lehmann T-N, Dehnicke C, Horn P, Nitsch R & Deisz RA (2010). Hyperpolarization-activated cation currents in the human epileptogenic neocortex. *Epilepsia* **51**, 404–414.

Williams JR & Payne JA (2004). Cation transport by the neuronal K^+-Cl^- cotransporter KCC2: thermodynamics and kinetics of alternate transport modes. *Am J Physiol Cell Physiol* **287**, C919–C931.

Wilson M & Gleason E (1991). An unusual voltage gated anion channel found in the cone of the chicken retina. *Vis Neurosci* **6**, 19–23.

Author contributions

The experiments were performed in the Electrophysiology Laboratory of the Institute of Cell Biology and Neurobiology, Center for Anatomy, Charité – Universitätsmedizin Berlin. R.A.D. designed the experiments, collected, analysed and interpreted the data, and wrote the manuscript. T.-N.L. provided the human tissues and critically revised the manuscript. P.H. provided some of the human tissues and made useful comments on the manuscript. C.D. cared for the patients, and provided clinical data and valuable comments on the manuscript. R.N. commented on the experimental design and the manuscript. All authors approved the final version for publication.

Acknowledgements

We are most grateful to S. Wierschke and Dr S. Gigout for valuable assistance during the experiments and valuable comments on the manuscript and to Dr L.A. Teichgräber for participating in the initial part of these experiments. We thank K. Mason for English proofreading. We are indebted to the Sonnenfeld Foundation for financial support of this project.